Title

Synthesis of Antibody-RNA Conjugates Targeting Amyloid Precursor Protein (APP) Knockdown in Basal Forebrain Cholinergic Neurons (BFCNs) to Treat Alzheimer's Disease (AD)

Author

Kwan, Yu Yan

Publication Date

2021

Peer reviewed|Thesis/dissertation

UNIVERSITY OF CALIFORNIA SAN DIEGO

Synthesis of Antibody-RNA Conjugates Targeting Amyloid Precursor Protein (APP) Knockdown in Basal Forebrain Cholinergic Neurons (BFCNs) to Treat Alzheimer's Disease (AD)

A Thesis submitted in partial satisfaction of the requirements

for the degree Master of Science

in

Biology

by

Yu Yan Kwan

Committee in charge:

Professor Steven F. Dowdy, Chair
Professor Susan Ackerman, Co-chair
Professor Yimin Zou

2021

The Thesis of Yu Yan Kwan is approved, and it is acceptable in quality and form for publication on microfilm and electronically.

University of California San Diego

2021

TABLE OF CONTENTS

LIST OF FIGURES

ACKNOWLEDGEMENTS

First, I would like to thank my thesis advisor, Steven F. Dowdy, who has provided patient guidance, encouragement and advice throughout my time as his student. You gave me a chance to learn everything I know about oligonucleotide therapeutics and my time in your lab has truly solidified my passion in this field. You have been everything I could have wanted in a mentor.

I would like to thank all the members of the Dowdy Lab, both past and present that I have worked with over the past two years. The Dowdy lab has been, and is, an incredible group of talented and creative people and this thesis would not have been possible without the contributions of a number of people. Special thanks to Ian Huggins, who recruited me to the lab when I was just an undergrad not knowing anything about antibody engineering or ARCs. Thank you for your mentorship and patiently teaching me all the skills and giving me so much advice and support whenever I needed. I would also like to thank: Satish Jadhav for the continuous supply of reagents and teaching me about nucleic acid chemistry; Ryan Setten for all the stimulating conversations; Xian-Shu Cui for keeping the Dowdy Lab running and taking care of all of us; and Carlos Medina for helping me with experiments when I had questions.

In addition, I would like to thank Dr. William Mobley for inviting me to his lab meetings to learn about neurobiology. I would also like to thank Aaron Johnstone for showing me all the *in vitro* work and patiently teaching me about neurobiology.

Last but not least, I would like to thank my family. I have been fortunate to have a close and loving family that has always given me their support in everything I have done. Thank you to my parents for your unconditional love and support and unshakable confidence in me. Thank you to my brother for listening and giving advice when I needed. Without the love and support of my family, I do not know where I would be.

Figure 3.5, “5C3-APP ARC by Lysine-Base Conjugation Internalizing into 3T3hTrkA Cells”; Figure 3.6, “5C3-APP ARC by Lysine-Based Conjugation Knocks Down APP in 3T3-

hTrkA Cells"; Figure 3.8, "5C3-MTG mAb Internalizing into 3T3-hTrkA Cells"; and Figure 3.13, "RTA-APP ARC by Lysine-Based Conjugation Internalizing into SY5Y-hTrkA Cells" were co-authored with Aaron Johnstone. The thesis author was the primary author of these figures.

ASO utilized was synthesized by Satish Jadhav. Linker peptide was synthesized by Xian-Shu Cui. Aaron Johnstone carried out all live internalization assays and knockdown assays.

ABSTRACT OF THE THESIS

Synthesis of Antibody-RNA Conjugates Targeting Amyloid Precursor Protein (APP) Knockdown in Basal Forebrain Cholinergic Neurons (BFCNs) to Treat Alzheimer's Disease

by

Yu Yan Kwan

Master of Science in Biology

University of California San Diego, 2021

Professor Steven F. Dowdy, Chair
Professor Susan Ackerman, Co-chair

Alzheimer's Disease (AD) is a devastatingly fatal neurodegenerative disease and a leading cause of dementia around the world. Despite the great medical need, none of the current FDA-approved AD drugs are disease-modifying. Based on a wealth of cell biological and pathological data, amyloid precursor protein (APP) overexpression is believed to contribute to

the degeneration of basal forebrain cholinergic neurons (BFCNs) in initiating AD pathogenesis. Therefore, we proposed that reducing APP expression in BFCNs would be a promising AD therapeutic strategy. Antisense oligonucleotides (ASOs) enable selective and potent degradation of target mRNA and are emerging as a powerful new tool for treating Central Nervous System (CNS) disorders. However, a targeting domain is needed to selectively deliver APP ASOs to BFCNs to prevent CNS-wide APP knockdown. To achieve this goal, I developed antibody-RNA conjugates (ARCs) that combine the superb specificity of anti-TrkA antibodies and the potency of APP ASOs to target APP knockdown in BFCNs.

To generate ARCs, I explored traditional lysine-based chemical conjugation and site-specific microbial transglutaminase (MTG) biochemical conjugation approaches, each required different antibody routes and conjugation chemistries. Lysine-based conjugation relied on random chemical conjugation through accessible lysines on the antibody surface. Although this approach was effective, it resulted in conjugate heterogeneity and a distribution of Drug:Antibody Ratios (DAR). To produce homogeneous DAR-2 ARCs, I explored site-specific MTG conjugation that targeted conjugation to the engineered tag at the antibody C-terminus. Together, my thesis outlined the framework for the development of ARCs that can be applicable to other neurological disorders.

1. Introduction

1.1 Alzheimer's Disease (AD)

Alzheimer's Disease (AD) is a devastating and progressive fatal neurodegenerative disease that affects a patient's memory and cognitive function. To date, AD impacts approximately 30 million people around the world and is the most common cause of dementia (Lane, Hardy, and Schott 2018). As worldwide population longevity increases, the number of AD patients is predicted to grow exponentially (Lane et al. 2018). Although there are currently some FDA-approved drugs to treat AD, none of these target the underlying genetic and molecular mechanism of the disease (Atri 2019). At best, these drugs only provide temporary symptomatic improvements by increasing the level of acetylcholine (ACh) in the brain, which is a neurotransmitter that is in short supply in the brain of AD patients (Chen and Mobley 2019). In other words, these drugs only delay the onset of AD symptoms, but do not stop the underlying destruction of neurons at the genetic level. Consequently, there is great medical need for a disease-modifying drug to treat AD.

A poorly understood but highly consistent feature of neurodegenerative disorders, termed Selective Neuronal Vulnerability, is that specific populations of neurons in the Central Nervous System (CNS) are at significantly high risk for synaptic dysfunction and death (Fu, Hardy, and Duff 2018). In AD, basal forebrain cholinergic neurons (BFCNs) are selectively vulnerable. Although BFCNs only account for 0.1% of CNS neurons, because of their widespread distribution of axons to cortex and hippocampus, they have a major role in regulating normal cognitive function in the brain (Schliebs and Arendt 2011). As a result, their degeneration or death significantly contributes to cognitive decline in AD (Chen and Mobley 2019).

Previous studies examining the loss of BFCNs in AD demonstrated that nerve growth factor (NGF) plays a role in their degeneration. NGF is an essential target-derived neurotrophic factor that binds and activates tropomyosin receptor kinase A (TrkA) receptor, which is robustly

expressed on the cell surface of BFCNs (Chen and Mobley 2019). Upon activation, NGF/TrkA signaling triggers downstream cellular pathways that are responsible for the survival, development and maintenance of BFCNs (Sofroniew, Howe, and Mobley 2001). A previous study by Capsoni et al. validated this concept by showing transgenic mice expressing high levels of neutralizing antibodies against NGF resulted in phenotypic changes similar to AD, including loss of BFCNs, abnormal amyloid precursor protein (APP) aggregates and behavior impairment (Capsoni et al. 2000). Thus, decreased level of NGF and disrupted NGF/TrkA signaling appear to be linked to BFCN loss in AD.

The question arises as to what causes the disruption of NGF/TrkA signaling that ultimately leads to the loss of BFCNs in AD. This question can be addressed by a Down Syndrome (DS) mouse model Ts65Dn (Salehi et al. 2006). These mice are segmentally trisomic for mouse chromosome 16, which is a homolog of human chromosome 21, and as a consequent they contain one extra copy of the APP gene, among other genes. APP is a type 1 transmembrane protein that is processed by sequential proteolytic cleavages via α- and β-secretases to shed Amyloid-Beta (Aβ) peptides varying in length (Thinakaran and Koo 2008). In fact, a wealth of genetic, cell biological and pathological studies of AD pointed out that Aβ peptides to be the initiation of AD pathogenesis (Selkoe and Hardy 2016).

In vivo experiments of Ts65Dn mice showed that increased APP gene expression resulted in phenotypes reminiscent of AD, including abnormal enlargement of early endosomes (EEs), decreased NGF retrograde transport in BFCNs, reduction in number and cell size of BFCNs, abnormal axonal distribution of BFCNs, and increased level of full-length APP (Salehi et al. 2006). Remarkably, when examining NGF transport in Ts65Dn mice, these mice achieved only about 4% level of NGF transport compared to controlled mice (Salehi et al. 2006). To further validate this concept, NGF transport was examined in Ts65Dn mice with only two copies of APP (Ts65Dn:APP $^{+/+/-}$) and they achieved about 50% of the level in control mice, showing

that decreasing APP expression in trisomic mice improved NGF transport (Salehi et al. 2006). Not surprisingly, when examining the correlation of APP expression level and BFCNs cell size, Ts65Dn:APP$^{+/+/+}$ mice showed significantly smaller BFCNs than Ts65Dn:APP$^{+/+/-}$ mice compared to control mice (Salehi et al. 2006). These findings established the correlation of APP overexpression and the disruption of NGF transport contributing to BFCN atrophy. Therefore, we proposed that the ability to restore APP to normal levels in BFCNs could potentially repair NGF retrograde transport and prevent BFCNs degeneration in AD.

1.2 Oligonucleotide Therapeutics

Oligonucleotide therapeutics are emerging as a powerful new tool for treating genetic diseases as RNA-targeting drugs (Crooke et al. 2018). Oligonucleotides, such as antisense oligonucleotides (ASOs) and short interference RNAs (siRNAs), are synthetic and chemically modified nucleic acids that interact with their target RNA sequence through Watson-Crick base-pairing. Depending on their mechanism of action, oligonucleotide therapeutics can alter gene expression by downregulating or upregulating target genes, altering mRNA splicing, targeting trinucleotide repeat disorders, expressing genes and editing genome (Dowdy 2017). In other words, oligonucleotide therapeutics have the ability to selectively drug the undruggable human genome that small molecules cannot access. Due to these unique characteristics, oligonucleotide therapeutics have the potential to treat human diseases ranging from cancer to pandemic outbreaks to CNS diseases (Dowdy 2017).

Recently, there was a preclinical study pursuing the use of splice-switching oligonucleotides (SSOs) to treat AD by inducing skipping of APP exon 17 that encodes the γ-secretase cleavage site and gives rise to Aβ42 peptide (Chang et al. 2018). Although *in vivo* treatment of mice with SSOs showed reduced level of Aβ42, the mechanism of action of SSOs is less efficient than ASOs that degrade their target mRNA by a Ribonuclease H (RNase H)-

dependent mechanism. More importantly, intracerebroventricular (ICV) administration led to widespread distribution of SSOs throughout the CNS, instead of targeting selectively vulnerable neurons (Chang et al. 2018). Since CNS-wide APP knockdown could lead to severe adverse cognitive defects, a viable therapeutic ASO needs to specifically target BFCNs for it to have relevance (Senechal et al. 2007).

1.3 ASOs to Treat AD

To address the AD neuron targeting problem, the focus of my project is to optimize delivery of APP ASOs to BFCNs via conjugation to anti-TrkA antibodies in the form of Antibody-RNA Conjugates (ARCs). Given their ability to recognize and bind antigens with superb specificity, antibodies offer an attractive tool as targeting domains to deliver ASOs to antigen-expressing cells (Perez et al. 2014). In fact, antibodies have been utilized for selective delivery of chemotherapeutics as Antibody-Drug Conjugates (ADCs) for nearly 20 years (Perez et al. 2014). By conjugating APP ASOs to anti-TrkA antibodies, I achieve two goals: 1) I directly impact selectively vulnerable BFCN neurons that play a significant role in AD, and 2) I specifically target APP knockdown in BFCN neurons instead of all neurons to avoid any possible toxic effects linked to decreased level of APP throughout the CNS.

ARC synthesis relies on effective conjugation of APP ASOs to the antibody without affecting its binding properties or pharmacokinetics (PK). Herein, I explored different chemical and biochemical conjugation strategies to produce ARCs, including lysine-based chemical conjugation and site-specific Microbial Transglutaminase (MTG) biochemical conjugation. Lysine-based conjugation first required the use of chemical linkers to activate lysine residues on the antibody surface by forming a stable amide bond, followed by conjugation to ASOs by copper-free strain-promoted azide-alkyne cycloaddition (SPAAC) click conjugation. Although this strategy was effective, it resulted in ARCs with poorly defined Drug:Antibody Ratios (DAR) because the conjugation reaction occurred randomly at any exposed lysine residues on the

antibody surface, leading to a heterogeneous mixture of ARCs with different numbers of ASOs attached at different positions throughout the antibody (Jain et al. 2015). Furthermore, uncontrolled ASO conjugation could interfere with antibody binding to antigen at the complementary determining regions (CDRs) as well as impact the PK profile (Sang et al. 2020).

An alternative conjugation strategy was the use MTG enzyme to yield site-specific conjugation. MTG belongs to a family of enzymes that catalyzes transamidation of the acyl group on glutamine side chains to the primary amine on lysine side chains (Strop 2014). This biochemical conjugation strategy required genetic engineering of the antibody to incorporate a highly selective and reactive glutamine handle for MTG recognition (Panowski et al. 2014). In contrast to lysine-based conjugation, implementation of MTG recognition sequence offers significant advantages of controlled conjugation sites and homogeneous products with a well-defined DAR. As a result, this strategy provides benefits of site-selective conjugation in terms of stability, manufacturing and improved therapeutic index (Farias et al. 2014).

Given the unique importance of APP overexpression and the significant role of BFCNs in AD, we proposed to knock down APP expression in BFCNs by developing TrkA-APP ARCs. Our work demonstrated that ARCs were produced successfully by both lysine- based and site-specific MTG conjugation strategies. *In vitro* experiments showed that ARCs bind to and internalize into TrkA expressing cells. Furthermore, APP levels were reduced in ARC-treated cells compared to untreated cells. Taking advantage of the targeting specificity of a TrkA antibody and the precision of ASOs to robustly degrade APP mRNA, we believe the development of ARCs has the potential to treat AD by targeting APP knockdown in selectively vulnerable BFCNs. Importantly, this work demonstrated the potential to specifically target the molecular mechanism of AD that no current FDA-approved AD drugs have pursued.

2. Materials and Methods

2.1 Antisense Oligonucleotides (ASO) Sequence and Synthesis

APP ASO sequence: 5'-TCACCGUUCTGCTGCATCUUGGA-3'. 5'-hexylamino-modified uniform phosphorothioate (PS) Gapmer ASO was synthesized with DNA phosphoramidites (A, C, G, T) and 2'-MOE modified RNA phosphoramidities for this study **(Fig 2.1)**. ASO synthesis was carried out at 1 umol scale using CPG UnyLinker solid support on a MerMade 6 oligonucleotide synthesizer (Bioautomation). Commercially available phosphoramidities (Glen Research) were used for synthesis according to manufacturer's recommendation. For 5'-hexylamino modification, a 0.1 M solution of 5'-Amino-Modifier C6 (Glen Research) in acetonitrile (ACN) containing 4-methoxytrityl (MMT) group protected amine. All solid support bearing ASOs were deprotected by treatment with aqueous NH_4OH at 55 °C for 18 hr. ASOs were purified by RP-HPLC on a 1200 Series HPLC (Agilent Technologies) with a Zorbax SB-C18 column (Agilent Technologies). ASOs were eluted with a linear gradient of ACN and fractions with absorbance at 260 nm were analyzed by MALDI-TOF mass spectrometry as well as denaturing Urea-PAGE gel (15% acrylamide, 7M Urea) followed by methylene blue staining. Fractions containing peaks with the correct mass were pooled, lyophilized, resuspended in 50% ACN/ 50% water and quantified by UV spectrophotometer.

2.2 ASO Treatment with Bicyclononyne-N-Hydroxysuccinimide Ester (BCN-NHS)

For all ASO treatments, BCN-NHS linker was reacted with ASO at the 5' amino group at a ratio of 10:1 **(Fig 2.2)**. Prior to reaction, ASO was lyophilized overnight to remove ACN. Lyophilized ASO was resuspended in sodium tetraborate buffer (pH 8.5) and added to a solution of BCN-NHS (10 mol equivalent) in DMSO. The reaction was incubated on a rotisserie at room temperature for 18 hr, followed by purification using HPLC Prep-C18 (Agilent Technologies). ASOs were eluted in a linear gradient running from 50 mM triethylammonium

acetate (TEAA) pH 7.0 in water to 90% ACN at a flow rate of 2 mL/min. Fractions with absorbance at 260 nm were analyzed by MALDI-TOF mass spectrometry as well as denaturing Urea-PAGE gel (15% acrylamide, 7 M Urea) followed by methylene blue staining. Fractions with the correct mass were pooled, lyophilized, resuspended in 50% ACN/50% water and quantified by UV spectrophotometer.

2.3 Mass Spectrometry

ASOs were analyzed by Voyager-DE PRO MALDI-TOF mass spectrometer (Applied Biosystems). 10 pmol of ASO was spotted with 2',4',6'-Trihydroxyacetophenone (THAP) matrix (Sigma-Aldrich, 91928). Spectra were collected in negative mode with accelerating voltage = 20,000V, grid = 90%, guide wire = 0.15%, 40 nsec delay time. About 300 shots were collected for each sample.

2.4 5C3 Monoclonal Antibodies (mAb) Production from Hybridoma Cells

Hybridoma cells were cultured in CD Hybridoma medium (Thermo Fischer Scientific), supplemented with GlutaMAX (Thermo Fischer Scientific) and Penicillin/Streptomycin (Thermo Fischer Scientific), in a humidified 37 °C tissue culture incubator with 8% CO_2 atmosphere. 30 mL cultures were grown in 125 mL vented shaker flasks (Thermo Fisher Scientific) on an orbital shaker set to 140 rpm. Cells were split when culture density reached approximately 2.0×10^6 cells/ mL – 3.0×10^6 cells/ mL by aspirating a portion of the culture and resuspending to a final density of 5.0×10^5 cells/mL with fresh pre-warmed culture medium. To harvest mAb, the cell suspension was centrifuged at 4500 × g for 20 min at 4 °C. The supernatant was filtered through 0.45 μm followed by 0.22 μm PVDF syringe filters. mAb was captured from the filtered supernatant by Protein A resins and eluted from the resins at low pH (pH 3.0) conditions. 1 uL of each elution fraction was run on a 10% reducing SDS-PAGE gel for characterization, followed

by UV protein staining (Gold Biotechnology) and imaging on a UV transilluminator. For the purposes of further purification and buffer exchange, eluted mAb was run through Size Exclusion Chromatography (SEC) on FPLC using an Enrich-SEC 650 10×300 column (Biorad, 780-1650) in phosphate buffered saline (PBS) with a flow rate of 1.8 mL/min. Fractions with absorbance at 280 nm containing mAb were pooled, concentrated by 30K Vivaspin ultrafiltration spin columns (Cytiva, 28932317), and quantified by UV spectrophotometer.

2.5 N-Hydroxysuccinimide Ester Azide (NHS-N_3) Antibody Labelling

For lysine-based conjugation, mAb was labelled with NHS-N_3 crosslinkers at the primary amines (-NH_2) in the side chain of lysine residues on the outer protein surface **(Fig 2.3)**. NHS-N_3 was dissolved in DMSO and reacted with mAb at a molar ratio of 10:1. Reactions were carried out in 0.1 M carbonate buffer to maintain a basic pH (pH 9.0) and incubated at 37 ^{o}C for 1 hr. Conjugation efficiency was analyzed by running 1 ug sample on a 10% reducing SDS-PAGE, followed by UV protein staining (Gold Biotechnology) and imaging on a UV transilluminator. Conjugated mAb was purified by SEC on FPLC using Enrich-SEC 650 10×300 column (Biorad, 780-1650) in PBS with a flow rate of 1.8 mL/min. Fractions with absorbance at 280 nm containing conjugated mAb were pooled, concentrated by 30K Vivaspin ultrafiltration spin columns (Cytiva, 28932317), and quantified by UV spectrophotometer.

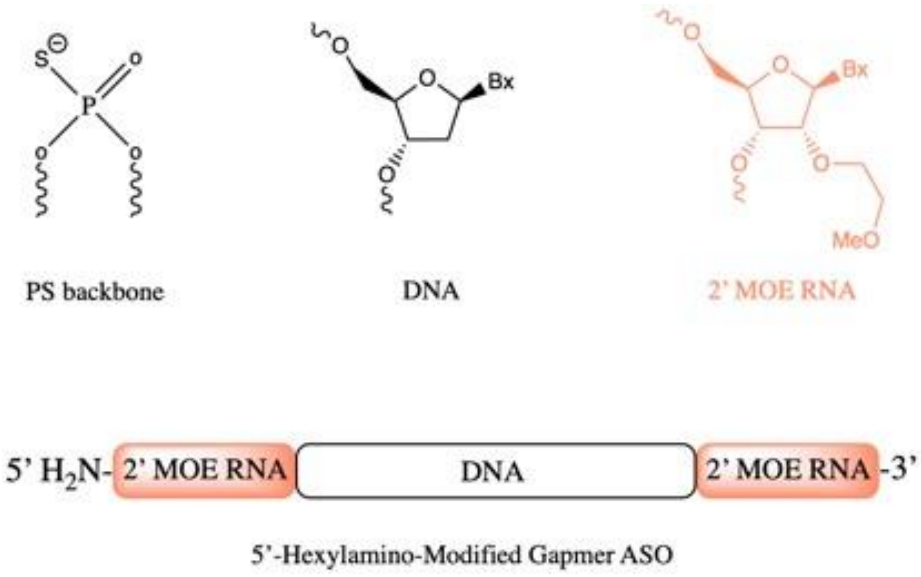

Figure 2.1. Gapmer ASO Design and Chemical Modifications.

Figure 2.2 General Scheme of BCN-NHS and 5'-Hexylamino-Modified APP ASO Reaction.

Figure 2.3 NHS-N_3 Reaction with Primary Amines in the Side Chain of Lysine Residues on the Antibody Surface.

2.6 Engineered 5C3-MTG Monoclonal Antibodies (mAb) Production

Heavy chain (HC) and light chain (LC) variable region sequences of an anti-TrkA mAb (5C3) were obtained from the original patent, synthesized as gBlocks (IDT), and codon optimized for the ExpiCHO expression system (Thermo Fischer Scientific). Particularly, a frameshift of the published 5C3 HC variable region protein sequence was discovered by comparing with other known sequences with high similarity to its framework. The sequence was corrected by introducing an E residue at the N-terminus and modifying the 7 last amino acids from "ILSHRLL" to "TSVTVSS" at the C-terminus **(Fig 2.4)**. Corrected HC and LC sequences were then seamlessly cloned into expression plasmids in frame with sequences encoding the appropriate constant regions (κ LC constant region and IgG1 HC constant region) using InFusion HD Reagent (Takara Bio USA, 639645). Microbial transglutaminase (MTG) conjugation handle (LLQGA) was cloned into the HC C-terminus followed by a translational termination by PCR-mediated mutagenesis. All sequences were confirmed by Sanger sequencing. Antibodies were produced by transfecting HC and LC expression plasmids in ExpiCHO cells (Thermo Fischer Scientific) at 1:1 HC:LC mass ratio according to manufacturer's recommendation. Cells were incubated in a humidified 37 ^{o}C incubator with 8% CO_2 on an orbital shaker set at 140 rpm. On the next day, cells were treated with ExpiFectamine CHO Enhancer (Thermo Fischer Scientific) and ExpiCHO Feed (Thermo Fischer Scientific) and transferred to a humidified 32^{o}C incubator with 5% CO_2 with shaking at 140 rpm. On day 5, additional ExpiCHO Feed was added according to manufacturer's protocol. Cell viability was monitored closely throughout the process and maintained above 70%. Antibody was harvested 12-14 days post-transfection. The cell suspension was collected and centrifuged at 200 × g for 5 min at 4 ^{o}C. The supernatant was then separated from the cell pellet and centrifuged again at 5000 × g for 30 min at 4 ^{o}C. The second supernatant was filtered through 0.45 μm followed by 0.22 μm PVDF syringe filters. Antibody was captured from the filtered supernatant by Protein A

resins and eluted from the resins at low pH (pH 3.0) conditions. 1 uL of each elution fraction was run on a 10% reducing SDS-PAGE gel for characterization, followed by UV protein staining (Gold Biotechnology) and imaging on a UV transilluminator. For the purposes of further purification and buffer exchange, eluted mAb was run through Size Exclusion Chromatography (SEC) on FPLC using an Enrich-SEC 650 10×300 column (Biorad, 780-1650) in phosphate buffered saline (PBS) with a flow rate of 1.8 mL/min. Fractions with absorbance at 280 nm containing mAb were pooled, concentrated by 30K Vivaspin ultrafiltration spin columns (Cytiva, 28932317) and quantified by UV Spectrophotometer.

2.7 Microbial Transglutaminase (MTG) Conjugation of 5C3-MTG mAb

For site-specific conjugations, 5C3-MTG mAb was conjugated to a lysine-azide bearing linker peptide (KP1Z) at the HC C-terminus engineered handle to yield 5C3-KP1Z with the use of MTG enzyme **(Fig 2.5)**. MTG reactions were carried out at a ratio of 40:1 (KP1Z: conjugation site). Antibody was added to the final concentration of 6.5 μM. 10X MTG enzyme buffer (500 mM Sodium Chloride, 500 mM Sodium Acetate, pH 5.8) was prepared and diluted to 1X in water. MTG enzyme was reconstituted in 1X MTG enzyme buffer to achieve a working concentration of 63 mg/mL. MTG enzyme was added to the reaction to achieve 25% of final volume. 10X MTG reaction buffer (1.5 M NaCl, 250 mM Tris-HCl, pH 8.0) was prepared and added to the reaction to achieve 1/10 the final reaction volume. Once 5C3-MTG mAb, KP1Z linker peptide, MTG enzyme and MTG reaction buffer were mixed well, the reaction was incubated at RT for 4 hr. Conjugation efficiency was analyzed by running 1 ug sample on a 10% reducing SDS-PAGE, followed by UV protein staining (Gold Biotechnology) and imaging on a UV transilluminator. ARCs were purified by SEC on FPLC using Enrich-SEC 650 10×300 column (Biorad, 780-1650) in PBS with a flow rate of 1.8 mL/min. Fractions with absorbance at

280 nm containing ARCs were pooled, concentrated by 30K Vivaspin ultrafiltration spin columns (Cytiva, 28932317), and quantified by UV spectrophotometer.

2.8 ARC Azide-Alkyne Click Conjugation

For ARC lysine-based conjugation, 5'-BCN-bearing ASO was conjugated to 5C3-NHS-N_3 via copper-free strain promoted azide-alkyne cycloaddition (SPAAC) click conjugation at a molar ratio of 3.5:1 (ASO:mAb) **(Fig 2.6)**. ASO was first dried down by vacuum evaporation and resuspended with 5C3-NHS-N_3 mAb in PBS and 40 mM L-Arginine. The reaction was incubated at 37 ^{o}C for 16 hr. For ARC site-specific conjugation, 5'-BCN-bearing ASO was conjugated to 5C3-KP1Z at a molar ratio of 4:1 (ASO:mAb). ASO was first dried down by vacuum evaporation and resuspended with mAb in PBS and 40 mM L-Arginine. The reaction was incubated at 30 ^{o}C for 16 hr. Conjugation efficiency was analyzed by running 1 ug sample on a 10% reducing SDS-PAGE, followed by UV protein staining (Gold Biotechnology) and imaging on a UV transilluminator. ARCs were purified by SEC on FPLC using Enrich-SEC 650 10×300 column (Biorad, 780-1650) in PBS with a flow rate of 1.8 mL/min. Fractions with absorbance at 280 nm containing ARCs were pooled, concentrated by 30K Vivaspin ultrafiltration spin columns (Cytiva, 28932317), and quantified by UV spectrophotometer.

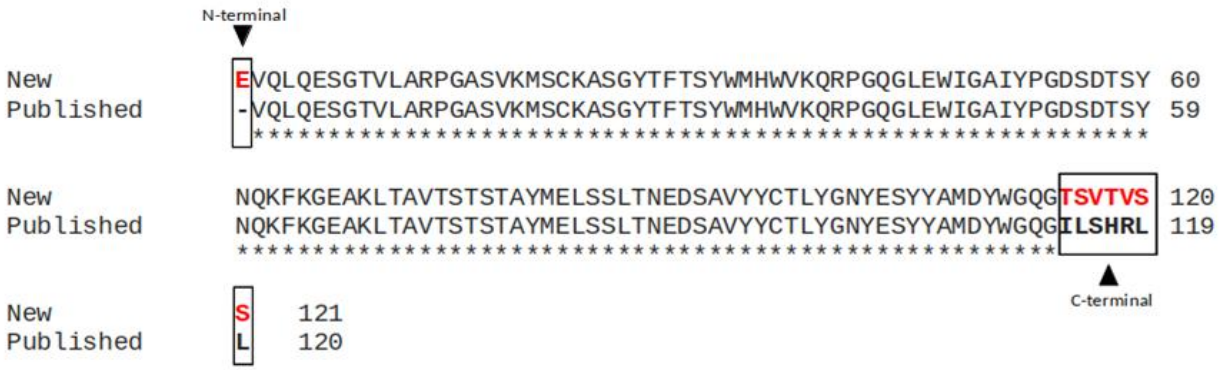

Figure 2.4 Comparison of the Corrected HC Variable Region Protein Sequence and the Original Published Sequence.

A

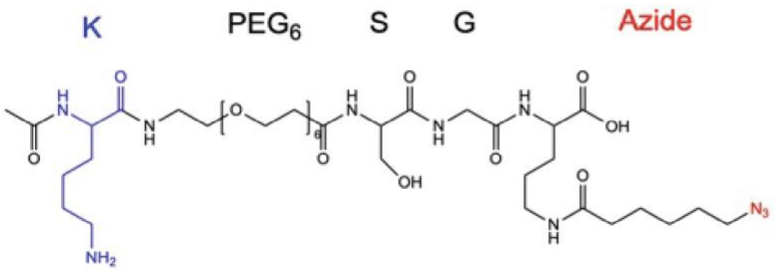

B

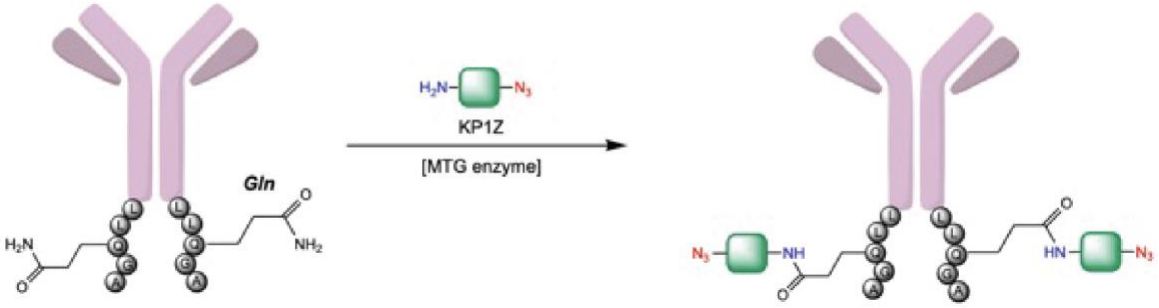

Figure 2.5 MTG Conjugation Reaction of 5C3-MTG mAb and KP1Z Linker Peptide. (A) Structure of KP1Z. **(B)** Glutamine side chain (acyl donor) reacts with primary amine (acyl acceptor) of KP1Z in MTG conjugation.

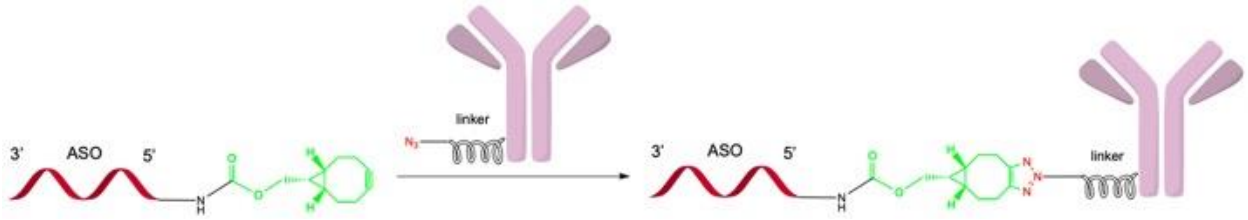

Figure 2.6 Copper-Free SPAAC Click Chemistry Reaction of 5' BCN-ASO and Linker Bearing Antibody.

2.9 Live Internalization Assays

Internalization of antibodies and ARC was assayed in 3T3 and SY5Y cells expressing human TrkA (hTrkA). Prior to antibody or ARC loading, live cells were washed with HBSS and chilled to 4 ºC on ice. Antibody or ARC were added at 50 nM and incubated at 4 ºC for 30 min then washed 3x with fresh, chilled HBSS. Cells were incubated for an additional 30 mins with anti-human, rabbit or mouse secondary antibody conjugated to AlexaFluor and then washed 3x with fresh, chilled HBSS. To allow internalization by endocytosis, cells were then warmed to 37 ºC to allow internalization and fixed with paraformaldehyde 4% and imaged with a widefield epifluorescence microscope.

2.10 APP Knockdown Assay by Western Blot

3T3-hTrkA cells were incubated for 6 days with 5C3 mAb, APP ASO, or ARC comprised of conjugated 5C3 and APP ASO at 50 nM. Cells were washed 3x with PBS and lysed in Laemmli sample buffer and proteins were separated by SDS-PAGE followed by immunoblotting with anti-APP and anti-Actin primary antibodies followed by HRP-conjugated secondary antibodies.

2.11 APP Knockdown Assay by Immunocytochemistry

3T3-hTrkA cells were incubated with 5C3 mAb, APP ASO, or ARC comprised of 5C3 conjugated to APP ASO at 50 nM for 5 days, then washed 3x with fresh PBS and fixed with paraformaldehyde 4% for 15 min. Fixed cells were washed 3x with fresh PBS and blocked/permeabilized with FBS 10% and Triton-X 0.3% in PBS for 1 hr at room temperature, and then incubated overnight at 4 ºC with anti-APP primary antibody. Cells were washed 3x with fresh PBS and incubated with AlexaFluor-labeled anti-mouse secondary antibody for 1 hour at

room temperature, and then washed 3x with fresh PBS, with the final wash containing DAPI nuclear stain. Cells were imaged with a widefield epifluorescence microscope.

2.12 Rabbit Polyclonal Antibodies (RTA) Production

RTA was obtained from Dr. William Mobley's lab. In brief, TrkA protein was first expressed by infection of Sf900 cells with TrkA-expressing baculovirus. TrkA proteins were purified from the supernatant by lentil lectin Sepharose column. Purified TrkA proteins were then injected to immunize rabbits to express RTA. RTA was purified from sera by Protein A affinity chromatography (Clary et al. 1994).

3. Results

3.1. Synthesis of 5'-BCN-bearing ASO

To functionalize the 5'-hexylamino-modified APP ASO for SPAAC click conjugation to antibodies, the ASO was first treated with Bicyclononyne-N-hydroxysuccinimide (BCN-NHS) to yield 5' BCN-bearing ASO **(Fig 3.1 A)**. To carry out this reaction, ASO was mixed with 10 mol equivalent of BCN-NHS reagent in a basic condition using sodium tetraborate buffer (pH 8.5). The reaction proceeded to completion overnight at room temperature. The conjugation progress was analyzed by running BCN-NHS-treated ASO alongside untreated ASO on a Urea-PAGE gel **(Fig 3.1 B)**. BCN-NHS-treated ASO displayed mobility shift compared to untreated ASO, indicating that the BCN group was conjugated to the ASO. RP-HPLC purification governed by polarity allowed effective separation of BCN-ASO (eluted at ~30 min) from excess BCN-NHS in the reaction by a linear gradient of acetonitrile (ACN), which is crucial for downstream conjugation to antibodies **(Fig 3.1 C)**. MALDI-TOF mass spectrometry analysis further demonstrated that the two fractions collected at 30 min contained BCN-ASO by showing a mass shift compared to untreated ASO of 172.49 m/z and 174.78 m/z, which is approximately the mass of a conjugated BCN group (178.1 m/z) **(Fig 3.1 D)**.

3.2. Lysine-Based Chemical Conjugation

3.2.1 Generation of TrkA mAbs from Hybridoma Cells

To generate ARCs by lysine-based conjugation, I produced 5C3 anti-TrkA monoclonal antibodies (mAbs) from hybridoma cells. Cells were cultured at 37°C for 5C3 expression. 5C3 contains IgG1 heavy chain (HC) constant region, therefore, Protein A resin was utilized for purification, since it avidly binds to the IgG Fc region. To purify 5C3, cells were pelleted and culture supernatant was filtered and passed through a Protein A chromatography column to capture 5C3 mAbs with no apparent loss in the flowthrough (Starting Material

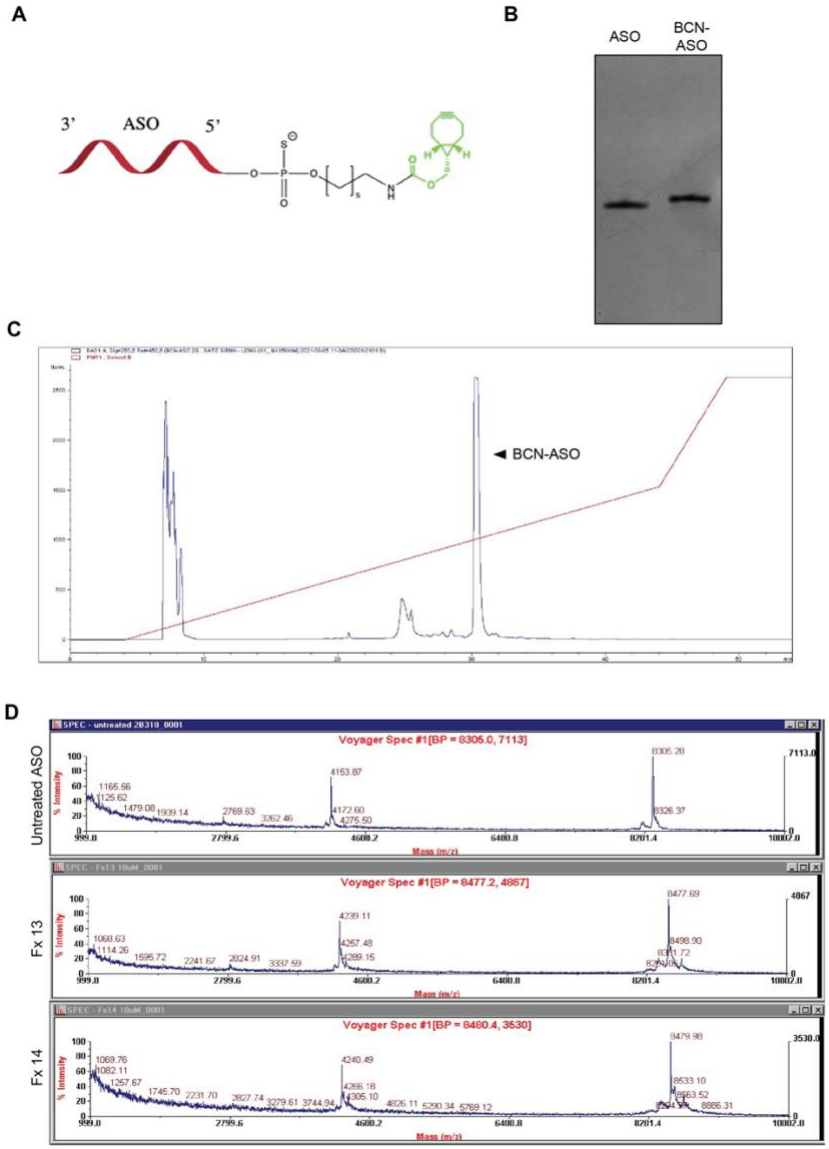

Figure 3.1 APP ASO and BCN-NHS Reaction and Purification. A) Structure of 5' BCN-bearing APP ASO. **B)** Methylene blue stained Urea-PAGE analysis of untreated ASO and BCN-ASO. **C)** RP-HPLC purification of BCN-ASO reaction. Labelled peak indicates elution of BCN-ASO. **D)** MALDI-TOF analysis of the two fractions collected in C compared to untreated ASO. Top panel – untreated ASO. Middle and bottom panels – elution fractions.

and Flowthrough) **(Fig 3.2 A)**. The resins were washed two times to remove all unwanted materials and proteins with no detectable loss of 5C3 mAb (Washes 1 and 2) **(Fig 3.2 A)**. pH 3.0 elution buffer was used to free captured 5C3 from Protein A resins, resulting in pure antibodies with HC (~50 kDa) and LC (~25 kDa) and no contaminants observed on SDS-PAGE gel (Elutions 1 and 2) **(Fig 3.2 A)**. To further purify 5C3 and buffer exchange to PBS, eluted 5C3 was run through FPLC SEC and no aggregates were observed in the final mAb product **(Fig 3.2 B)**. Yields varied between batches and cell passages, but typically ranged from 400 – 700 ug per 30 mL culture.

3.2.2 Conjugation of 5C3 mAbs and NHS-N_3 Crosslinker

To conjugate 5C3 mAb to BCN-ASO, 5C3 was first functionalized with NHS-N_3 crosslinkers at the primary amine side chain of lysine residues on the antibody surface. Following a 1 hr incubation at 37 °C of a 10:1 molar ratio of NHS-N_3 to 5C3, SDS-PAGE analysis showed a single band of HC and LC with increased molecular weights compared to untreated 5C3, demonstrating both HC and LC were efficiently labelled with NHS-N_3 crosslinkers in the reaction **(Fig 3.3 A)**. To separate conjugated 5C3-N_3 from excess NHS-N_3, the reaction was run through FPLC SEC in PBS **(Fig 3.3 B)**. SEC cleanly separated the two molecules in different fractions as larger molecules (5C3-N_3) eluted before smaller molecules (NHS-N_3). Fractions containing only pure 5C3-N_3 conjugates (13-15 mL) were collected for downstream ASO conjugation.

3.2.3 Generation of ARC by SPAAC Click Chemistry

ARC was generated by SPAAC click conjugation of 5C3-N_3 and BCN-ASO **(Fig 3.4 A)**. The azide group of NHS-N_3 on 5C3 lysine residues allows conjugation to the BCN group at the 5’ end of APP ASO, resulting in triazole formation **(Fig 3.4 A)**.

To optimize the reaction to generate ARC with an average of DAR 2, different molar ratios of BCN-ASO to 5C3-N_3 ranging from 1:1 to 5.5:1 were tested at a small scale **(Fig 3.4 B)**. Following a 16 hr incubation at 37 °C, SDS-PAGE analysis revealed that higher molar ratios resulted in more complete conversion of HC-N_3 to HC-N_3-BCN-ASO and a larger distribution of ASOs per antibody **(Fig 3.4 B).** Importantly, each additional HC-N_3-BCN-ASO band displayed a molecular weight shift of approximately 8 kDa, which was consistent with the molecular weight of an APP ASO, indicating one additional ASO per HC for each shift **(Fig 3.4 B)**. Among all tested molar ratios, 3.5:1 showed the most conjugated HC and the most DAR 2 species (1 ASO per HC) without too many DAR >2 species (>1 ASOs per HC) as observed in 4.5:1 and 5.5:1 **(Fig 3.4 B)**. The results aligned with our prediction that any lysine residues on the antibody surface could be labelled by NHS-N_3 and conjugated to BCN-ASO, resulting in uncontrolled ASO conjugation to the antibody. Hence, this conjugation approach led to a distribution of DAR.

To achieve a DAR 2 average, I scaled up the conjugation reaction with 3.5:1 molar ratio, resulting in a distribution of DAR 2-8 (1-4 ASOs per HC) with mostly DAR 2 species (1 ASO per HC) **(Fig 3.4 C)**. To separate ARCs from free BCN-ASO, the rection was run through FPLC SEC in PBS **(Fig 3.4 D)**. SEC cleanly separated the two molecules as ARC eluted before free BCN-ASO in different fractions **(Fig 3.4 D)**. Importantly, FPLC SEC analysis showed one single peak (13-15 mL) corresponding to ARC, indicating no aggregates or degraded species **(Fig 3.4 D)**.

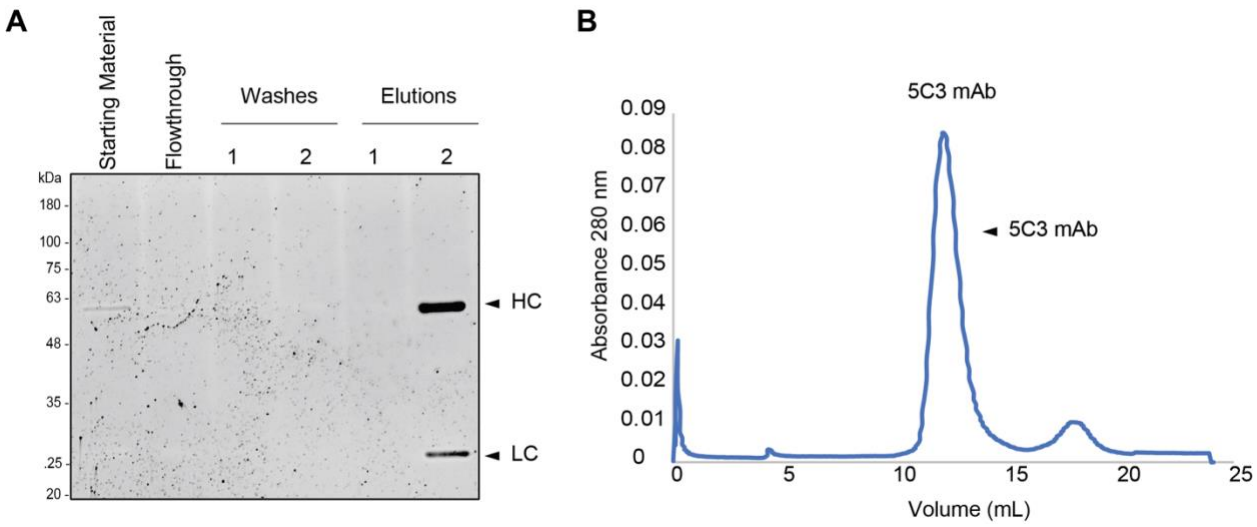

Figure 3.2 5C3 mAb Production and Purification from Hybridoma Cells. A) 10% Reducing SDS-PAGE analysis of protein A fractions revealed supernatant (starting material) contains IgG heavy chain (HC) bands (50 kDa) and light chain (LC) bands (25 kDa). Flowthrough revealed depletion of antibody. Wash fractions did not contain any antibodies. Elution fraction 2 contains all antibodies. **B)** FPLC SEC purification of 5C3 mAb with absorbance at 280 nm showed a pure sample with no aggregates or contaminants.

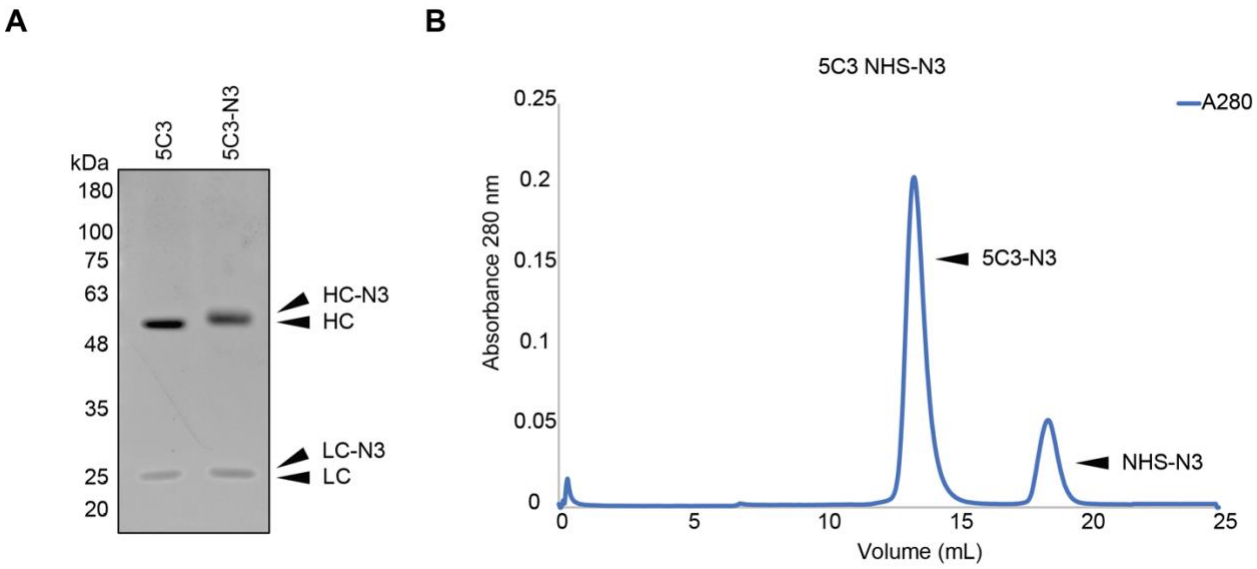

Figure 3.3 5C3 NHS-N_3 Conjugation and Purification. A) 10% Reducing SDS-PAGE gel of untreated 5C3 and 5C3-N_3 conjugate. Molecular weight markers are in kilodaltons (kDa). HC – heavy chain, LC – Light chain, HC-N3 – heavy chain-NHS-N3 conjugate, LC-N3 – light chain-NHS-N3 conjugate. **B)** FPLC SEC purification of 5C3-N_3 conjugate from excess NHS-N_3.

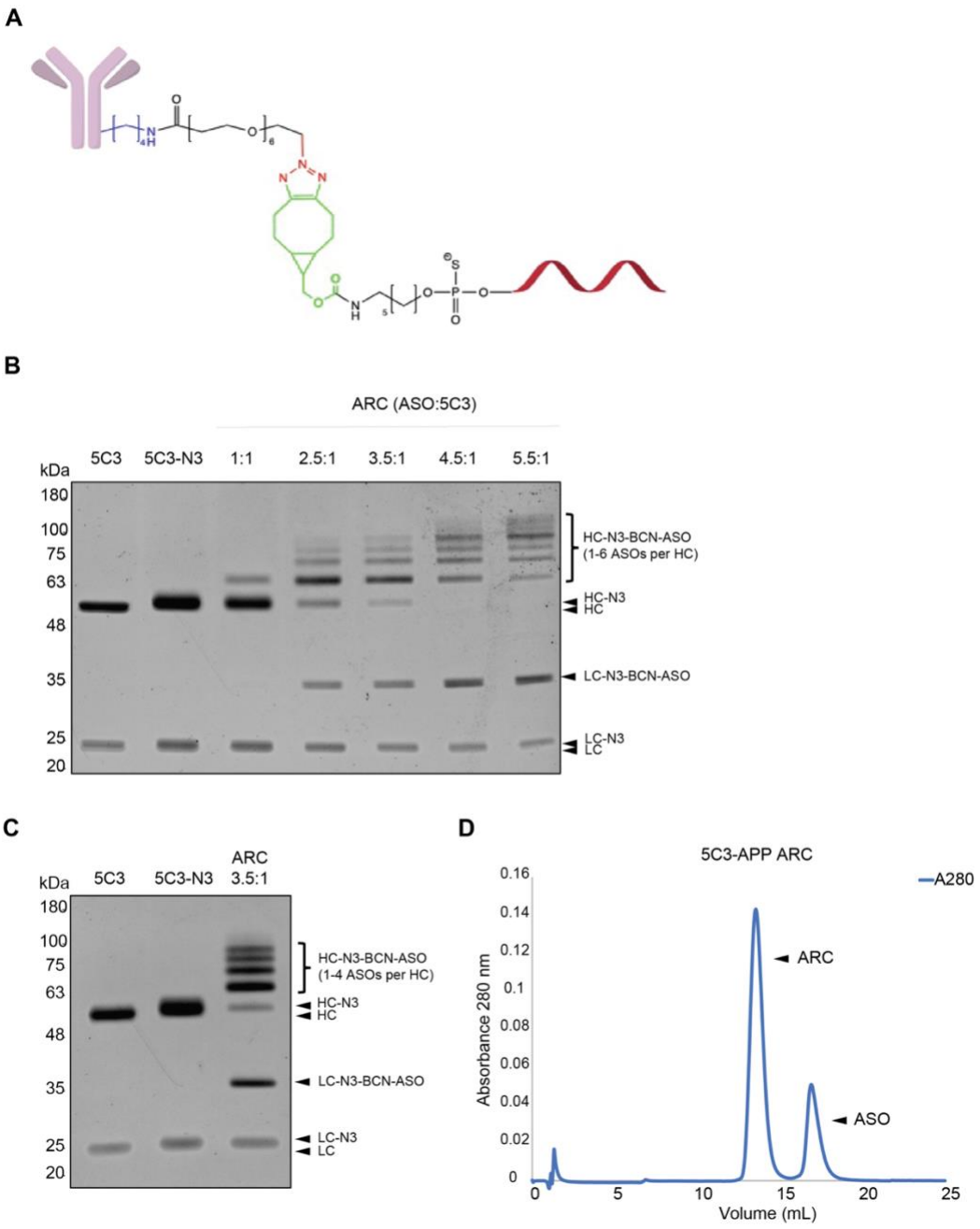

Figure 3.4 Lysine-Based Conjugation and Purification of 5C3-APP ARC. A) Structure of 5C3-N_3-BCN-ASO ARC. Conjugated lysine is highlighted in blue. Conjugated triazole is highlighted in red. Conjugated BCN is highlighted in green. **B)** 10% Reducing SDS-PAGE analysis of ASO:5C3 molar ratio optimization to produce ARCs with an average of DAR 2. Molecular weight markers are in kilodaltons (kDa). HC – heavy chain, LC – Light chain, HC-N3 – heavy chain-NHS-N3 conjugate, LC-N3 – light chain-NHS-N3 conjugate, HC-N3-BCN-ASO – heavy chain-NHS-N3-BCN-ASO conjugate, HC-N3-BCN-ASO. **C)** 10% Reducing SDS-PAGE gel of untreated 5C3, 5C3-N3 and 3.5:1 ARC scale-up reaction. **D)** FPLC SEC purification of ARC from excess ASO.

3.2.4 ARC Binding to Human TrkA (hTrkA)-Positive Cells

Conjugation of ASOs to mAbs may interfere with their binding avidity. To test whether lysine-based conjugation altered 5C3 binding functionality, we treated hTrkA-expressing 3T3 cells with ARCs to examine if they internalized and accumulated in cells like 5C3 mAb alone **(Fig 3.5)**. We observed robust uptake and trafficking to intracellular foci in each case, indicating that ARCs with average DAR 2 generated by lysine-based conjugation did not interfere with antibody binding.

3.2.5 ARC *In Vitro* Knockdown Test

Conjugation of macromolecules like antibodies to ASOs can alter their ability to induce knockdown response. To test whether ARC was able to achieve APP knockdown in 3T3-hTrkA cells, we treated 3T3-hTrkA cells with 5C3 mAb, APP ASO and ARC and examined their APP protein expression by immunocytochemistry **(Fig 3.6 A)**. Untreated control and 5C3-treated 3T3-hTrkA expressing cells showed similar level of APP signal, indicating 5C3 mAb alone did not reduce APP protein expression **(Fig 3.6 A)**. In contrast, treatment with APP ASO and ARC showed reduced APP protein expression compared to control and 5C3-treated cells **(Fig 3.6 A)**. These results suggested that conjugation of an antibody to an ASO did not interfere with its induction to target mRNA knockdown.

To further examine whether protein knockdown was specific to APP in 3T3-hTrkA cells, we treated the cells with 5C3 mAb, APP ASO and ARC and examined their APP protein level relative to actin level by Western Blot **(Fig 3.6 B)**. Similar to the immunocytochemistry results, untreated control and 5C3-treated 3T3-hTrkA cells showed similar APP protein expression while APP ASO- and ARC-treated 3T3-hTrkA cells showed reduced expression **(Fig 3.6 B)**. However, actin level was relatively similar across all samples, suggesting that knockdown activity was highly specific to APP mRNA **(Fig 3.6 B)**. Taken together, *in vitro* treatment of 3T3-hTrkA cells with 5C3 mAb, APP ASO and ARC revealed ARC was able to achieve APP knockdown in cells

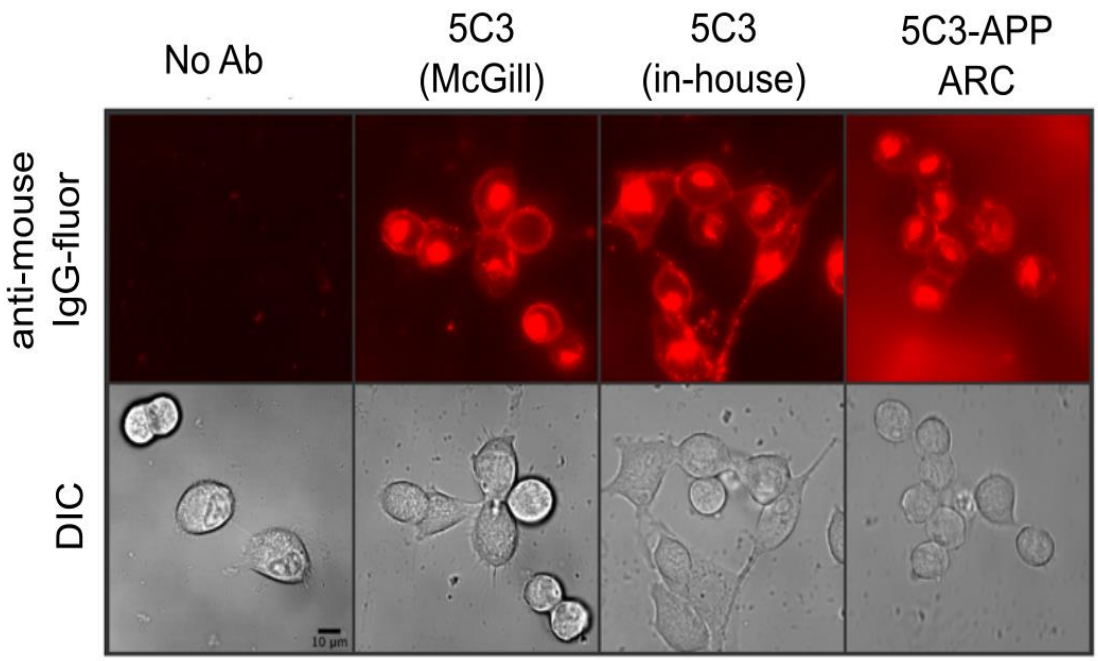

Figure 3.5 5C3-APP ARC by Lysine-Based Conjugation Internalizing into 3T3-hTrkA Cells. 3T3-hTrkA cells were treated with no antibodies (control), 5C3 obtained from our collaborator at McGill University, 5C3 generated by our lab, and ARC.

A

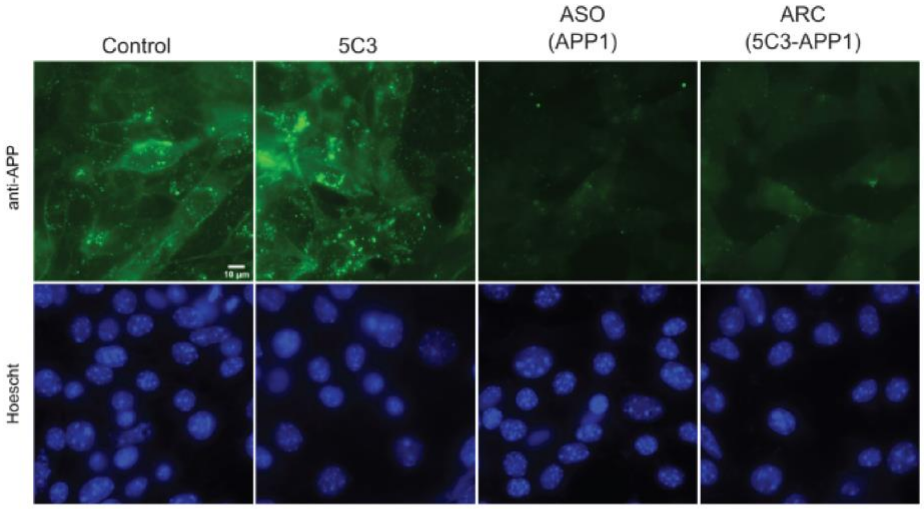

B

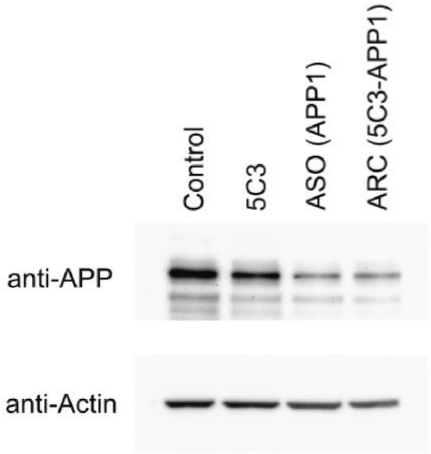

Figure 3.6 5C3-APP ARC by Lysine-Based Conjugation Knocksdown APP in 3T3-hTrkA Cells. A) Immunocytochemistry of APP protein signal of control, 5C3-, ASO- and ARC-treated cells. Reduced APP signal was observed in ASO- and ARC-treated cells. **B)** Western blot analysis of APP protein level of control, 5C3-, ASO-, ARC-treated cells. Reduced APP protein relative to actin controls was observed in ASO- and ARC-treated cells.

as unconjugated APP ASO. More importantly, conjugation of an antibody to an ASO did not alter its ability to induce mRNA knockdown.

3.3 Site-Specific MTG Biochemical Conjugation

3.3.1 Generation of Engineered TrkA mAbs

Lysine-based conjugation strategy allowed ASOs to conjugate to any lysine residues on the antibody surface, resulting in ARCs with heterogeneous DARs and possible interference of the antibody binding site. To address this problem and improve ARC design, we modified 5C3 HC sequence and engineered a microbial transglutaminase (MTG) conjugation tag at the C-terminus for site-specific conjugation.

Previously, our lab attempted to engineer 5C3 based on the published sequence of the original patent and express it from ExpiCHO cells, but it did not successfully yield antibody. After careful examination and comparing 5C3 sequences with other known antibody sequences with high similarity to its framework, we made a hypothesis that the published 5C3 sequence contained a frameshift at the HC variable region, hence disrupting protein folding and inhibiting expression from ExpiCHO cells. To test this hypothesis, we corrected the HC variable region sequence by introducing an E residue at the N-terminus and altered the last 7 amino acids at the C-terminus. Synthetic cDNAs encoding LC and corrected HC variable regions were cloned upstream of appropriate constant regions (Kappa LC, IgG1 HC) into expression plasmids. The MTG conjugation tag (LLQGA) was inserted at the C-terminus of HC constant region for site-specific conjugation, followed by translational termination. ExpiCHO cells were transfected with a 1:1 ratio of HC to LC expression plasmids, incubated at 37 °C overnight followed by 32 °C for 12-14 days for mAb expression.

To purify 5C3-MTG mAbs, transfected ExpiCHO cells were pelleted, the culture supernatant was filtered and then passed through a Protein A chromatography column, allowing

capture of antibodies and flowthrough of unwanted proteins in the culture media (Starting Material and Flowthrough) **(Fig 3.7 A)**. The resins were washed two times with no loss of antibodies (Washes 1 and 2) **(Fig 3.7 A)**. Pure 5C3-MTG mAbs with HC (50 kDa) and LC (25 kDa) were eluted from resins under low pH (pH 3.0) and collected in fraction 2 (Elutions 1-3) **(Fig 3.7 A).** To further purify eluted mAbs and buffer exchange into PBS, elution fraction 2 was run through FPLC SEC **(Fig 3.7 B)**. Fractions containing mAb aggregates (10-11 mL) were removed and only fractions with pure 5C3-MTG mAb (12-15 mL) were collected **(Fig 3.7 B)**. This prevented mAb aggregation and precipitation in downstream conjugation reactions. Yields varied between batches, but typically ranged from 400-600 ug per 35 mL culture.

Our result supported our hypothesis that the published 5C3 sequence in the original patent contained a frameshift, hindering expression from ExpiCHO cells. More importantly, it demonstrated that correcting the HC variable region sequence rescued expression of 5C3-MTG mAb in ExpiCHO cells, allowing us to proceed with site-specific conjugation.

3.3.2 5C3-MTG mAbs Binding to hTrkA-Positive Cells

To test whether 5C3-MTG mAb sequence modifications affected the antibody binding and internalization properties, we performed an internalization assay using 3T3-hTrkA cells **(Fig 3.8)**. Cells were incubated with recombinant 5C3-MTG mAb or original 5C3 mAb expressed by hybridoma cells at 4 °C for 30 min, followed by fluorescent secondary antibody incubation. Anti-mouse secondary antibody was used to recognize original 5C3 mAb and anti-human secondary antibody was used to recognize 5C3-MTG mAb as it contained a human IgG1 backbone. The result revealed that 5C3-MTG mAb was internalized and accumulated in 3T3-hTrkA cells as the original 5C3 mAb, verifying the sequence modifications did not affect the antibody binding and internalization functionalities.

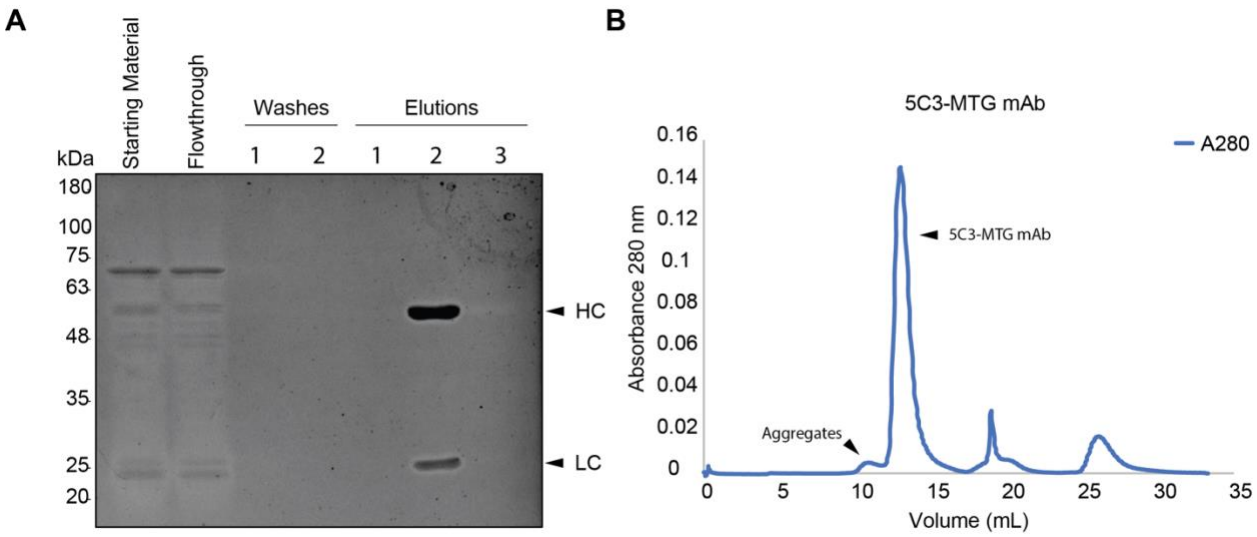

Figure 3.7 Engineered 5C3-MTG mAb Production and Purification from ExpiCHO Cells. **A)** 10% Reducing SDS-PAGE analysis of protein A fractions revealed supernatant (starting material) contains IgG heavy chain (HC) bands (50 kDa) and light chain (LC) bands (25 kDa). Flowthrough revealed depletion of antibody bands. Wash fraction did not contain any antibodies. Elution fractions 2 contains all antibodies. **B)** FPLC SEC purification of 5C3-MTG mAb with absorbance at 280 nm showed the sample contained some aggregates. Only the fractions containing pure 5C3-MTG mAb (12-15 mL) were collected.

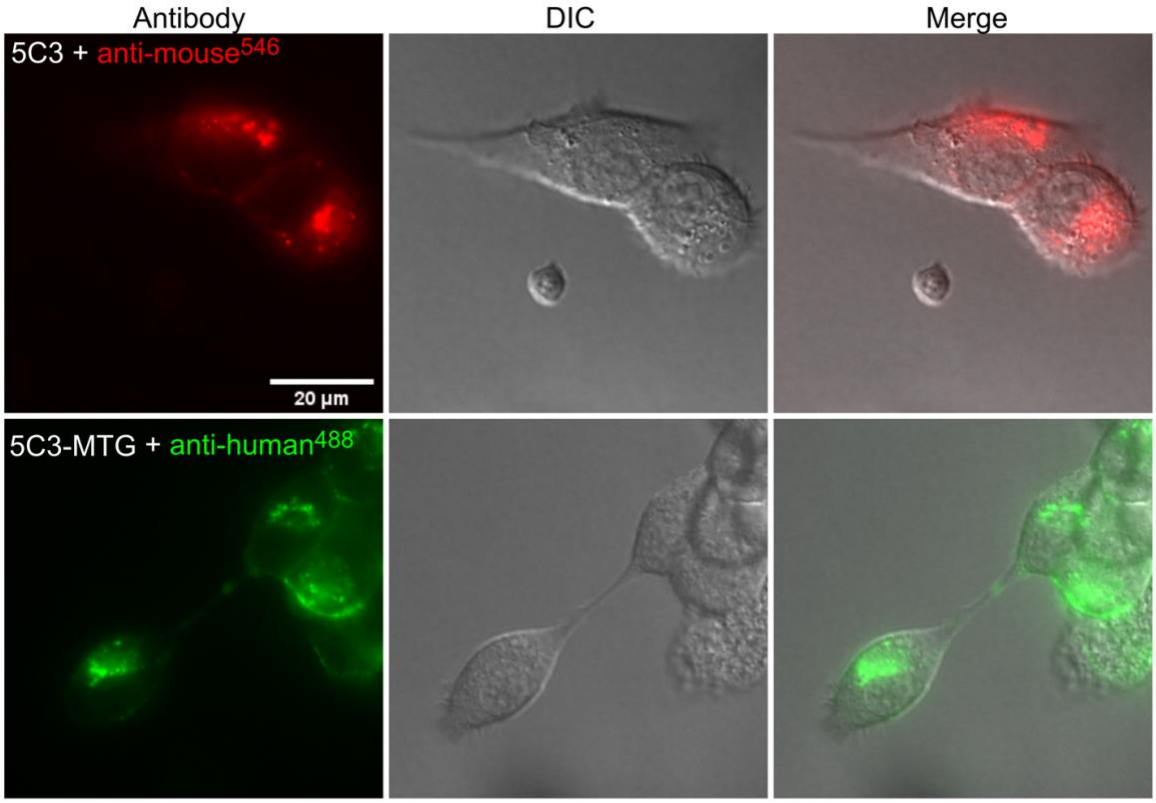

Figure 3.8 5C3-MTG mAb Internalizing into 3T3-hTrkA Cells. Anti-mouse secondary antibody was used recognize original 5C3 mAb (top panels) and anti-human secondary antibody was used to recognize 5C3-MTG mAb (lower panels).

3.3.3 MTG Conjugation of 5C3-MTG mAbs and Linker Peptide

To conjugate 5C3-MTG mAb to BCN-ASO, 5C3-MTG mAb was first conjugated to a bi-functionalized Lysine-Azide bearing linker peptide (KP1Z) **(Fig 3.9 A)**. KP1Z allowed for MTG conjugation to 5C3-MTG mAb at the C-terminal engineered glutamine residue via the lysine amino group, thus allowing SPAAC click conjugation with BCN-ASO via the azide group. To optimize MTG conjugation reaction, 20:1 and 40:1 molar ratios of KP1Z to conjugation site (CS) (2 CSs per mAb) and 60-240 min of incubations were tested at small scales **(Fig 3.9 B)**. SDS-PAGE analysis revealed that KP1Z recognized and targeted conjugation to the engineered MTG tag (LLQGA) at the HC C-terminus **(Fig 3.9 B)**. Only one single band was observed for LC at 25 kDa, and this result further validated that KP1Z was specific to the MTG tag at HC C-terminus **(Fig 3.9 B)**. Among all tested molar ratios and incubation times, HC was most conjugated to KP1Z (HC-KP1Z) with a molar ratio of 40:1 incubated for 240 min **(Fig 3.9 B)**. As a result, 5C3-KP1Z was produced at a large scale under this condition **(Fig 3.9 C)**. Impressively, SDS-PAGE analysis showed a nearly complete conversion to 5C3-KP1Z with no LC conjugation **(Fig 3.9 C)**. To separate conjugated 5C3-KP1Z from free KP1Z and MTG enzyme, the rection was run through FPLC SEC in PBS **(Fig 3.9 D)**. SEC cleanly separated three molecules and allowed them to elute in different fractions. SEC analysis also revealed that there were some aggregates (13 mL), thus only the fractions containing pure 5C3-KP1Z conjugates (14 – 16 mL) were collected **(Fig 3.9 D)**.

3.3.4 Generation of ARC by SPAAC Click Chemistry

ARC was generated by copper-free SPAAC click conjugation of 5C3-KP1Z and BCN-ASO **(Fig 3.10 A)**. The azide group of KP1Z linker peptide allowed conjugation to the BCN group at the 5’ end of ASO, resulting in triazole formation **(Fig 3.10 A)**.

To maximize conjugation, different incubation temperatures (RT, 30 °C and 37 °C) were tested with a 4:1 molar ratio of ASO to mAb for 16 hr at small scales **(Fig 3.10 B)**. SDS-PAGE analysis revealed that BCN-ASO was conjugated to 5C3-KP1Z at all temperatures **(Fig 3.10 B)**. As the temperature increased, the intensity of the HC-KP1Z-ASO band increased while the HC-KP1Z band decreased, indicating more ASOs were conjugated to the mAb **(Fig 3.10 B)**. Furthermore, HC-KP1Z-ASO conjugate displayed an apparent shift of approximately 8 kDa, consistent with conjugation of 1 ASO per HC. This result indicated site-specific generation of defined DAR 2 ARCs **(Fig 3.10 B)**. In addition, LC did not display any molecular weight shift in all cases, demonstrating BCN-ASOs conjugated specifically to KP1Z linker peptides that were conjugated to the engineered MTG tag at the HC C-terminus **(Fig 3.10 B)**. However, a trace amount of antibody aggregates with a molecular weight of 75 kDa were observed at 37 °C, which was approximately the molecular weight of HC-LC aggregates **(Fig 3.10 B)**. To prevent aggregation, we decided to carry out ARC production with a 4:1 molar ratio of ASO to mAb at 30 °C for 16 hr incubation **(Fig 3.10 C)**. SDS-PAGE analysis revealed that there was no protein aggregation under this condition **(Fig 3.10 C)**. There was an approximate 70 – 80% conversion of HC-KP1Z conjugate to HC-KP1Z-ASO conjugates **(Fig 3.10 C)**. The reaction was run through FPLC SEC to separate ARCs from excess BCN-ASO, and SEC analysis further validated that there were no antibody aggregates in the reaction as only one single peak of ARC (13-15 mL) was observed **(Fig 3.10 D).**

3.4 Generation of ARC with Rabbit Polyclonal Antibodies (RTA)

3.4.1 Conjugation of RTA and NHS-N_3 Crosslinker

RTA-APP ARC was generated by lysine-based conjugation. To conjugate RTA to ASO, RTA was first functionalized with NHS-N_3 crosslinkers at the primary amines (- NH_2) of lysine residues on the antibody surface **(Fig 3.11 A)**. Following a 1 hr incubation at 37 °C of a 20:1

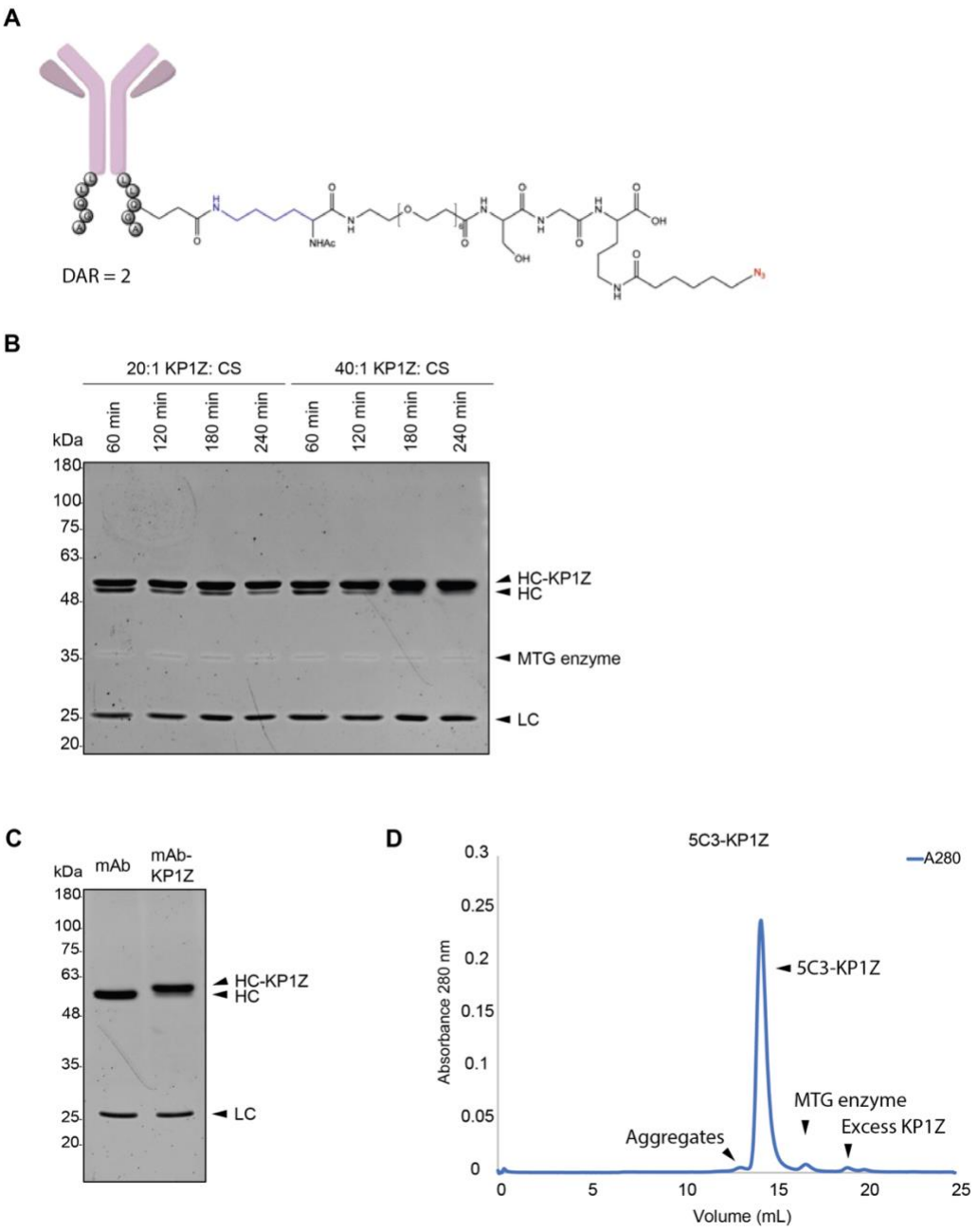

Figure 3.9 5C3-KP1Z Conjugation and Purification. A) Structure of 5C3-KP1Z conjugate. Conjugated lysine is highlighted in blue. Conjugatable azide of KP1Z linker peptide for SPAAC click conjugation is highlighted in red. **B)** 10% Reducing SDS-PAGE analysis of KP1Z:CS molar ratio and incubation time optimization to produce 5C3-KP1Z conjugate. Molecular weight markers are in kilodaltons (kDa). CS – conjugation site, HC – heavy chain, LC – Light chain, HC-KP1Z – heavy chain-KP1Z conjugate, MTG enzyme – microbial transglutaminase enzyme. **C)** 10% Reducing SDS-PAGE analysis of large-scale production of 5C3-KP1Z with 40:1 molar ratio of KP1Z to CS and 240 min incubation. **D)** FPLC SEC purification of 5C3-KP1Z from MTG enzyme and KP1Z linker peptide.

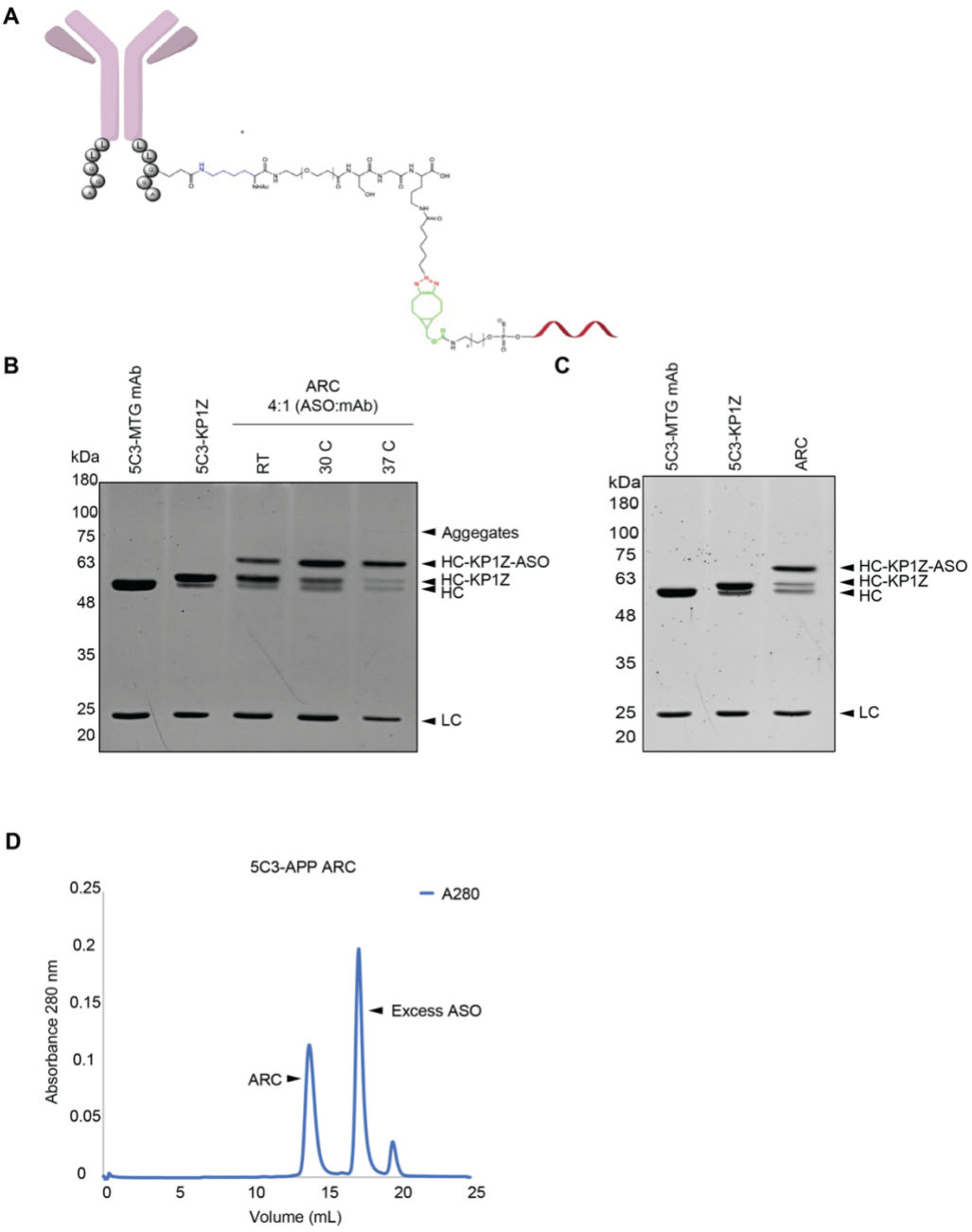

Figure 3.10 Site-Specific MTG Conjugation and Purification of 5C3-APP ARC. A) Structure of 5C3-KP1Z-BCN-ASO structure. Conjugated lysine is highlighted in blue. Conjugated triazole is highlighted in red. Conjugated BCN is highlighted in green. **B)** 10% Reducing SDS-PAGE analysis of ARC produced with a 4:1 molar ratio of ASO to mAb at room temperature (RT), 30 °C and 37 °C for 16 hr. Molecular weight markers are in kilodaltons (kDa). HC – heavy chain, LC – Light chain, HC-KP1Z – heavy chain-KP1Z conjugate, HC-KP1Z-ASO – heavy chain-KP1Z-ASO conjugate. **C)** 10% Reducing SDS-PAGE gel of 5C3-MTG mAb, 5C3-KP1Z and 4:1 30 °C ARC scale-up reaction. **D)** FPLC SEC purification of ARC from excess ASO.

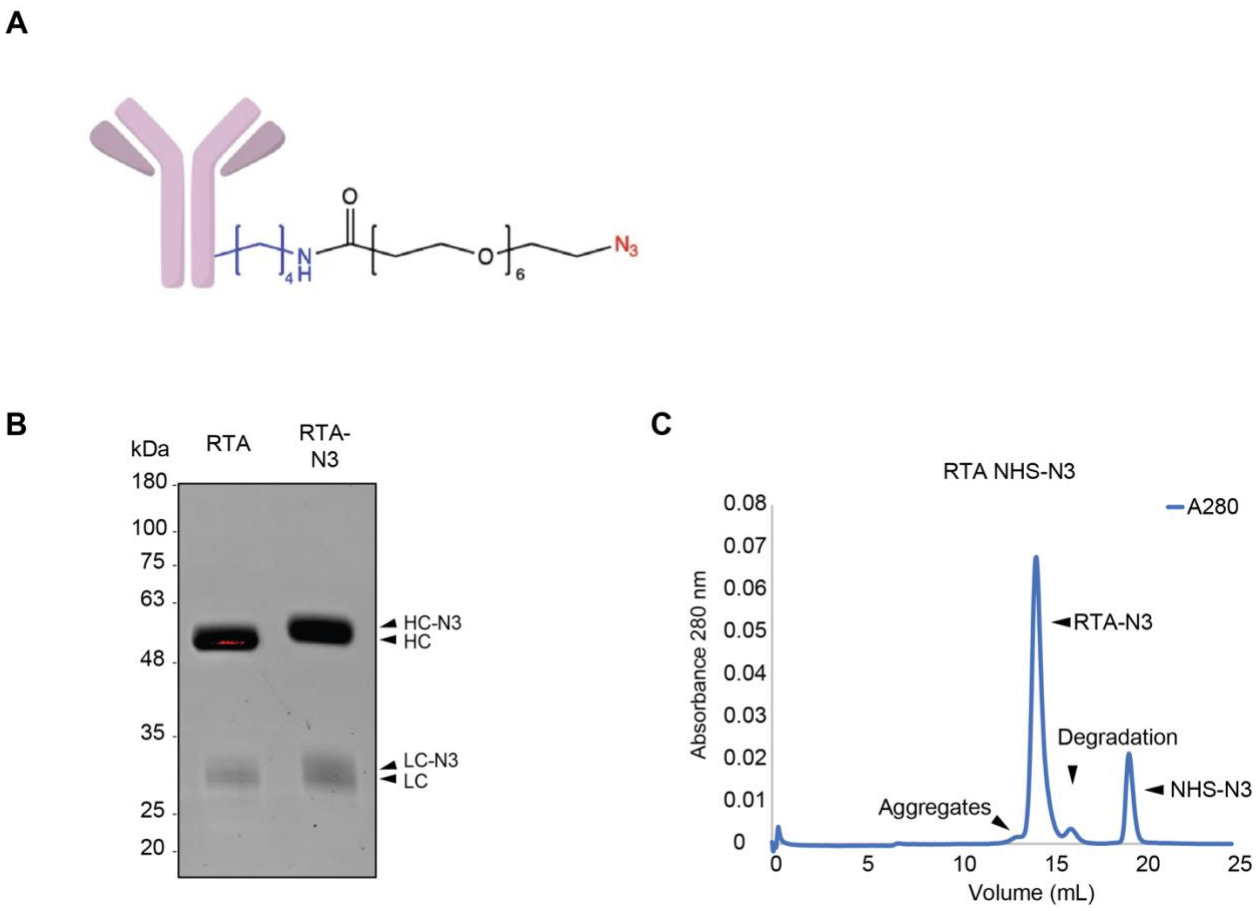

Figure 3.11 RTA NHS-N_3 Conjugation and Purification. A) Structure of RTA-N_3 conjugate. Conjugated lysine is highlighted in blue. Conjugatable azide group of NHS-N_3 linker for SPAAC click conjugation is highlighted in red. **B)** 10% reducing SDS-PAGE gel of untreated RTA and RTA-N_3. Molecular weight markers are in kilodaltons (kDa). HC – heavy chain, LC – light chain, HC-N3 – heavy chain-NHS-N_3 conjugate, LC-N3 – light chain-NHS-N_3 conjugate. **C)** FPLC SEC purification of RTA-N_3 conjugate from excess NHS-N_3.

molar ratio of NHS-N_3 to RTA, SDS-PAGE analysis revealed a single band of HC and LC with increased molecular weights compared to untreated RTA, indicating both HC and LC were labelled with NHS-N_3 crosslinkers in the reaction **(Fig 3.11 B)**. To separate conjugated RTA-N_3 from excess NHS-N_3, the reaction was run through FPLC SEC in PBS **(Fig 3.11 C)**. SEC cleanly separated the two molecules and allowed them to elute in different fractions **(Fig 3.11 C)**. In addition, SEC analysis revealed some aggregation (13 mL) and degradation (16 mL) of RTA **(Fig 3.11 C)**. As a result, only the fractions containing pure RTA-N_3 (14-15 mL) were collected **(Fig 3.11 C)**.

3.4.2 Generation of ARC by SPAAC Click Chemistry

RTA-N_3 was conjugated to BCN-ASO via copper-free SPAAC click conjugation to generate RTA-APP ARC **(Fig 3.12 A)**. The azide group of NHS-N_3 on RTA lysine residues allowed conjugation to the BCN group at the 5' end of ASO, resulting in triazole formation **(Fig 3.12 A)**.

To yield RTA-APP ARCs with an average of DAR 2, the conjugation reaction was optimized by testing different molar ratios of BCN-ASO to RTA-N_3 ranging from 2.5:1 to 4:1 at a small scale. Following a 16 hr incubation at 37 °C, SDS-PAGE analysis revealed that higher ratios of ASO to RTA resulted in more complete conversion of HC-N_3 to HC-N_3-BCN-ASO and a larger distribution of ASOs per antibody **(Fig 3.12 B)**. Each additional HC-N_3-BCN-ASO band displayed an approximate 8 kDa molecular weight shift, consistent with the molecular weight of one ASO, indicating one additional ASO per HC for each shift **(Fig 3.12 B)**. Among all tested molar ratios, 3.5:1 showed that most conjugated HC and the most DAR 2 species (1 ASO per HC) without too many DAR >2 species (>1 ASOs per HC) as seen in 4:1 **(Fig 3.12B)**.

To achieve RTA-APP ARCs with an average of DAR 2, I scaled up the conjugation reaction with 3.5:1 molar ratio, resulting in an approximate distribution of DAR 2-6 (1-3 ASOs

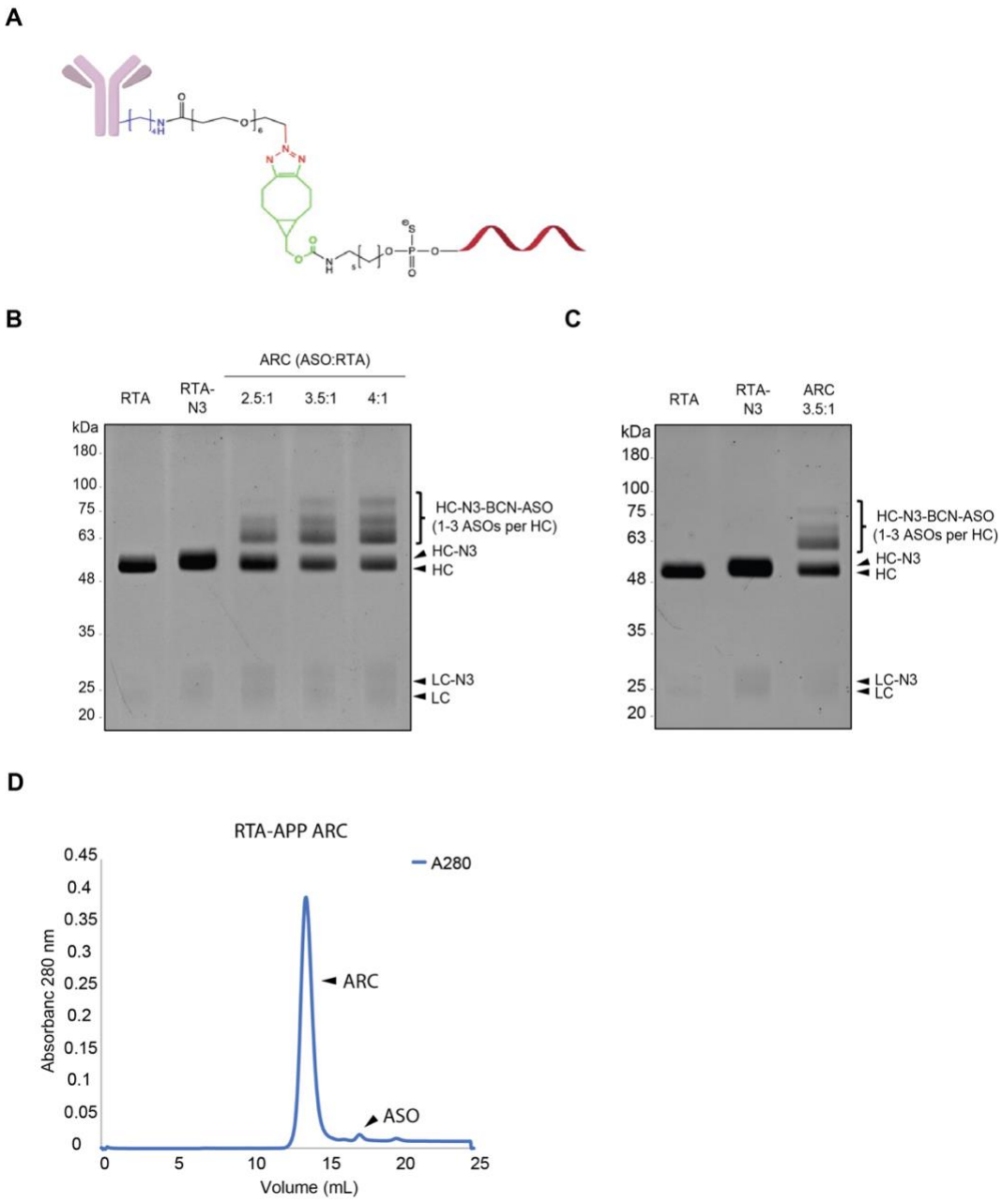

Figure 3.12 Lysine-Based Conjugation and Purification of RTA-APP ARC. A) Structure of RTA-N_3-BCN-ASO ARC. Conjugated lysine is highlighted in blue. Conjugated triazole is highlighted in red. Conjugated BCN highlighted in green. **B)** 10% Reducing SDS-PAGE analysis of ASO:RTA molar ratio optimization to ARCs with an average of DAR 2. Molecular weight markers are in kilodaltons (kDa). HC – heavy chain, LC – light chain, HC-N_3 – heavy chain-NHS-N_3 conjugate, LC-N3 – light chain-NHS-N_3 conjugate, HC-N3-BCN-ASO – heavy chain-NHS-N_3-BCN-ASO conjugate. **C)** 10% Reducing SDS-PAGE gel of untreated RTA, RTA-N3 and 3.5:1 ARC scale-up reaction. **D)** FPLC SEC purification of RTA-APP ARC from excess ASO.

per HC) with mostly DAR 2 species (1 ASO per HC) **(Fig 3.12 C)**. To separate ARC from free BCN-ASO, the rection was run through FPLC SEC in PBS **(Fig 3.12 D)**. SEC cleanly separated the two molecules as ARC eluted before free BCN-ASO in different fractions **(Fig 3.12 D)**. Importantly, FPLC SEC analysis showed one single peak corresponding to ARC, indicating no antibody aggregates or degraded species **(Fig 3.12 D)**.

3.4.3 ARC Binding to hTrkA-Positive Cells

To test whether RTA-APP ARC retained antibody binding and internalization functionalities to hTrkA-expressing cells, we performed an internalization assay using SY5Y-hTrkA cells **(Fig 3.13)**. Both untreated control cells and ARC-treated cells were treated with anti-rabbit secondary antibody to visualize binding and internalization **(Fig 3.13)**. This result revealed that RTA-APP ARCs bound to and internalized into SY5Y-hTrkA cells, demonstrating conjugation of ASO did not alter RTA binding avidity.

Acknowledgements

Figure 3.5, “5C3-APP ARC by Lysine-Base Conjugation Internalizing into 3T3hTrkA Cells”; Figure 3.6, “5C3-APP ARC by Lysine-Based Conjugation Knocks Down APP in 3T3-hTrkA Cells”; Figure 3.8, “5C3-MTG mAb Internalizing into 3T3-hTrkA Cells”; and Figure 3.13, “RTA-APP ARC by Lysine-Based Conjugation Internalizing into SY5Y-hTrkA Cells” were co-authored with Aaron Johnstone. The thesis author was the primary author of these figures.

ASO utilized was synthesized by Satish Jadhav. Linker peptide was synthesized by Xian-Shu Cui. Aaron Johnstone carried out all live internalization assays and knockdown assays.

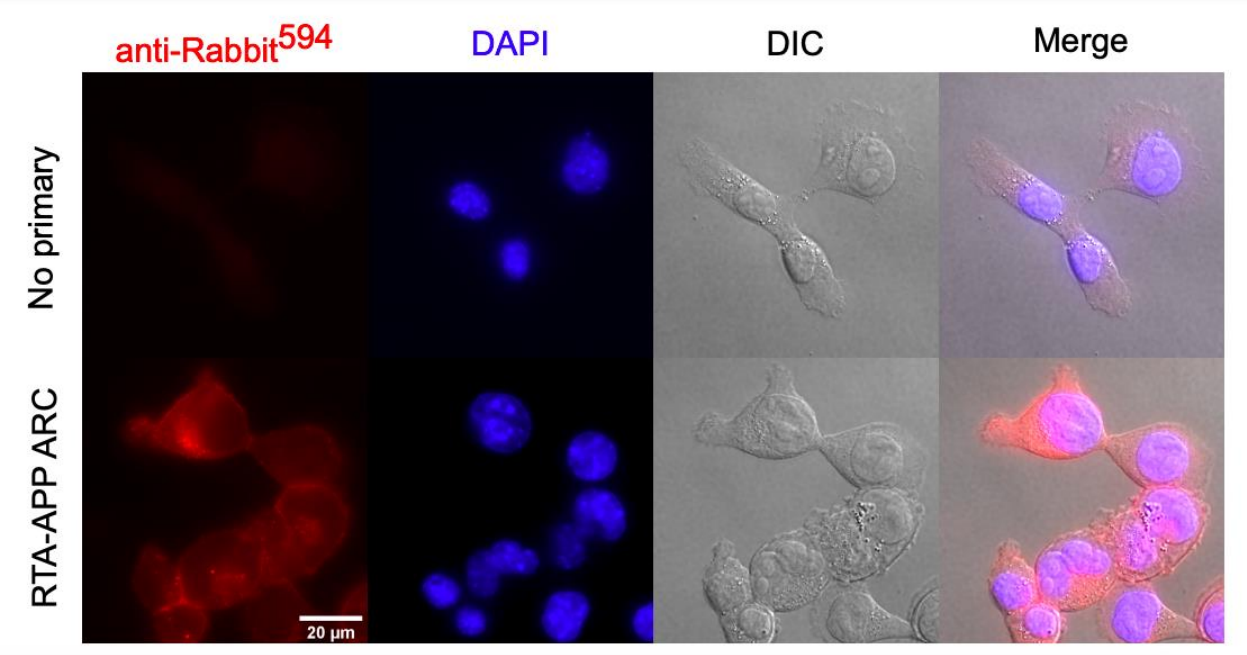

Figure 3.13 RTA-APP ARC by Lysine-Based Conjugation Internalizing into SY5Y-hTrkA Cells. Cells were treated with no primary antibodies (top panel) or RTA-APP ARC (lower panel). Anti-rabbit secondary antibodies were used to visualize binding and internalization.

4. Discussion

4.1 Introduction

Alzheimer's Disease (AD) is a devastatingly fatal neurodegenerative disease and a leading cause of dementia around the world. Although there are currently FDA-approved drugs to treat AD, they only provide temporary symptomatic improvements and none of these address the underlying molecular mechanism of the disease. Based on a wealth of cell biological and pathological data, APP overexpression is believed to contribute to the synaptic dysfunction and degeneration of BFCNs in initiating AD pathogenesis (Capsoni et al. 2000; Chen and Mobley 2019; Salehi et al. 2006; Schliebs and Arendt 2011; Selkoe and Hardy 2016). Therefore, we proposed that reducing APP expression in selectively vulnerable BFCNs would be a promising AD therapeutic approach.

Oligonucleotide therapeutics, including siRNAs and ASOs, have the potential to treat a wide range of human diseases from cancers to pandemic outbreaks to CNS diseases (Dowdy 2017). Due to their superb specificity for their target sequence, oligonucleotide therapeutics have the potential to drug the undruggable human genomes that small-molecule therapeutics cannot access (Dowdy 2017). In addition, they can pharmaco-evolve to keep pace with genetic mutations of human diseases. Despite these potentials, the major hurdles to overcome to fully achieve their utilities is targeting delivery. In my thesis work, I applied these principles in designing and generating TrkA-APP ARCs that target APP knockdown in BFCNs selectively.

4.2 Generation of ARCs to Treat AD

To improve the potency and pharmacological properties of APP ASOs, our lab synthesized Gapmer APP ASOs with full PS backbone and 2'-MOE modifications **(Fig 2.1)**. The incorporation of PS backbone at all DNA gap and RNA flanking regions enhances nuclease resistance and promotes ASO binding to plasma proteins, thus reducing clearance and

improving drug pharmacokinetics (Roberts, Langer, and Wood 2020). 2'-MOE modifications at both RNA flanking regions also further improves ASO stability by enhancing binding affinity to the target mRNA (Kole, Krainer, and Altman 2012; Roberts et al. 2020). Furthermore, the amino moiety ($-NH_2$) synthesized on the 5' end of our ASOs allows for treatment with BCN-NHS for SPAAC click conjugation with antibodies.

ASOs can be taken up by cells through endocytosis and slowly enter the cytoplasm or nucleus to induce RNase H-dependent mRNA knockdown activity (Dowdy 2017). However, CNS-wide APP knockdown would lead to severe adverse cognitive defects. To enhance APP ASO delivery specifically to BFCNs in the CNS, a targeting domain was conjugated to APP ASOs. Antibodies possess exquisite specificity to their target antigens, and they have been utilized for selective delivery of ADC chemotherapeutics for over 20 years (Perez et al. 2014). Therefore, antibodies provided an attractive tool to target BFCNs in the CNS. In my thesis work, TrkA antibodies were conjugated to APP ASOs in the form of Antibody-RNA Conjugates (ARCs), thus directly addressing the BFCNs targeting problem.

To generate TrkA-APP ARCs, I explored traditional random lysine-based chemical conjugation and site-specific MTG biochemical conjugation, each required different antibody production routes and linker chemistries. To pursue lysine-based conjugation, 5C3 TrkA mAbs were effectively produced by hybridoma cells and purified through Protein A affinity chromatography. In general, traditional conjugation strategies were limited to the use of the side chains of amino acids on the antibody surface, including the amino group (NH_2) of lysine and the sulfhydryl group (SH) of cysteine (Jain et al. 2015). Utilizing lysine residues on 5C3 mAb surface, I demonstrated the use of NHS-N_3 chemical linkers that allowed copper-free SPAAC click conjugation with BCN-ASO to form ARCs. SDS-PAGE analysis revealed higher molar ratios of ASOs to mAbs resulted in more ASOs conjugated per mAb, leading to a larger distribution of DARs. To achieve an average of DAR 2, a 3.5:1 molar ratio was utilized for large-scale production. Our *in vitro* studies suggested that ARCs generated by lysine-based

conjugation were internalized to 3T3-hTrkA cells. Also, immunocytochemistry and western blot analysis showed reduced APP level relative to actin level in ARC-treated 3T3-hTrkA cells, demonstrating conjugation to antibodies did not affect APP ASO-induced knockdown activity and target specificity.

Although lysine-based conjugation strategies were effective, the disadvantage was a mixture of heterogeneous DARs. As ASOs were conjugated to any accessible lysines on the antibody surface, it was impossible to control the conjugation sites. This feature may interfere with mAb binding and will also result in significant batch-to-batch variation that impairs drug pharmacokinetics and clearance. Applying these lessons to improve the design of ARCs, I explored site-specific MTG biochemical conjugation strategy. First, 5C3 mAb was genetically engineered to contain an MTG conjugation handle (LLQGA) at the heavy chain C-terminus, and the antibody was efficiently expressed using the ExpiCHO expression system. MTG enzyme catalyzed conjugation of a bi-functional lysine-azide bearing linker peptide (KP1Z) to the engineered handle site-specifically through a transamidation reaction. *In vitro* internalization assays using 3T3-hTrkA cells demonstrated the sequence modifications did not alter antibody binding avidity. Importantly, SDS-PAGE analysis revealed an efficient and near complete MTG conjugation of KP1Z to the heavy chains but not light chains, validating MTG conjugation was site-specific to the engineered handles at the heavy chains C-termini. Conjugation of mAb-KP1Z and BCN-ASO was carried out by SPAAC click chemistry. To maximize ARC yield while avoiding antibody aggregation, the incubation temperature was optimized to 30 °C. Together, this design allowed consistent generation of ARCs with well-defined DAR of 2. The engineered handles at the heavy chains C-termini ensured site-specific conjugation and prevented interference of antibody binding, thus avoided the pitfalls of traditional chemical conjugation.

4.3 Future Directions

Overall, my thesis work demonstrated the production of TrkA-APP ARCs with DAR 2 through lysine-based chemical conjugation and site-specific MTG biochemical conjugation approaches. Construction of ARCs is highly modular and requires different components. Future studies are focused on implementations of advances in each of the field of antibody production, linker chemistry and oligonucleotide chemistry to enhance targeting specificity, solubility and potency. Most ASOs in pre-clinical and clinical trials contain full PS backbone and extensive 2' modifications to improve stability, delivery, and binding avidity to target RNA (Juliano 2016). Other than 2'-MOE, other chemical modifications at the 2' position of the ribose sugar are commonly used to increase nuclease resistance and improve the stability of ASOs, including 2'-O-methyl (OMe) and 2'-Fluoro (2'-F) (Hammond et al. 2021; Roberts et al. 2020). An even greater binding affinity chemistry to target RNA can be achieved by bridged nucleic acids (BNAs), which are types of nucleotides that contain a methyl bridge between the 2'-O and 4' positions of the ribose sugar (Roberts et al. 2020). For example, 2'-O-ethyl (cEt) BNAs can be incorporated to the RNA flanking regions of Gapmer ASOs to increase binding affinity to target mRNA, thus reducing the length of ASO. As such, cEt 3-10-3 gapmers are more efficacious than MOE 5-10-5 gapmers and smaller to improve delivery (Roberts et al. 2020). cEt is excluded from the DNA gap region as it enhances binding to RNA, thus it is not compatible with RNase H-mediated cleavage. Overall, these recent advances in chemical modifications of oligonucleotides aid delivery by improving stability and binding avidity.

Targeting APP ASO delivery to BFCNs required the use of TrkA antibodies. However, the yield and quality differences between batches could bottleneck production. To improve mAb production and increase yield, optimizations could be focused on the antibody construct design and the cell system. Screening of new TrkA mAbs may also allow for more selective binding and productive internalization pathways. In addition, culture conditions can be further optimized to increase transfection efficiency and yields.

My work demonstrated the highly selective and controlled production of ARCs with DAR 2; however, these conjugation approaches can be applied to produce ARCs with higher or lower DARs. For example, by incorporating MTG conjugation handles on both HCs and LCs, ARCs with DAR 4 can be produced. Also, smaller mAb derivatives, such as fragment antigen-binding (Fab) and single chain variable fragments (scFv) can be used as alternatives to full mAbs to generate ARCs with DAR 1. Previous studies have shown that Fab derived from a full transferrin mAb successfully targeted siRNA delivery in muscular tissues (Sugo et al. 2016). Also, scFvs were demonstrated to exhibit great *in vivo* stability and improved binding avidity compared to full mAbs (Colcher et al. 1990). These studies illustrated that smaller mAb derivatives could be attractive alternatives to intact mAbs to target delivery.

ARCs discussed here utilized non-cleavable linkers that only allowed release of APP ASO from the conjugate following complete lysosomal degradation of mAb after internalization. An alternative to non-cleavable linkers is to use cleavable linkers that allow release of ASOs under specific conditions, such as protease-sensitivity, pH-sensitivity and glutathione sensitivity (Jain et al. 2015). Protease-sensitive linkers take advantage of dominant proteases in target cells to recognize and cleave specific peptide sequences, such as valine-citrulline linkers that are cleaved by Cathepsin B upon internalization by target cancer cells (Jain et al. 2015). pH-sensitive linkers, such as hydrazone linkers, utilize the change of pH levels in the endosomes (pH 5-6) and lysosomes (pH 4.8) compared to the cytoplasm (pH 7.4) to release cytotoxins (Jain et al. 2015). Glutathione-sensitive linkers are reducible disulfide linkers that take advantage of high concentrations of glutathione in the endosomal and lysosomal compartments to release cytotoxins (Jain et al. 2015). Although cleavable linkers are primarily used to clinically improve ADCs, these same linkers could potentially enhance ASO delivery by allowing more rapid release of ASOs from mAbs and increase APP knockdown activity.

4.4 Conclusion

My thesis work described here outlined the framework for the development of TrkA-APP ARC to target AD pathogenesis that no current FDA-approved AD drugs pursued. Taking advantage of the exquisite specificity of TrkA mAbs and the potency of APP ASOs, I achieved two goals: 1) I directly impacted the selectively vulnerable BFCNs that play a significant role in AD, and 2) I specifically targeted APP knockdown in BFCNs instead of CNS-wide neurons to avoid possible toxic effects linked to reduced APP expression throughout the CNS. The modularity of ARCs allows implementations of advances of each component to enhance potency. Importantly, the technology herein could be broadly applicable to treat other selectively vulnerable neurons in other neurological disorders.

References

Atri, Alireza. 2019. “Current and Future Treatments in Alzheimer’s Disease.” *Seminars in Neurology* 39(2):227–40. doi: 10.1055/s-0039-1678581.

Capsoni, Simona, Gabriele Ugolini, Alessandro Comparini, Francesca Ruberti, Nicoletta Berardi, and Antonino Cattaneo. 2000. “Alzheimer-like Neurodegeneration in Aged Antinerve Growth Factor Transgenic Mice.” *Proceedings of the National Academy of Sciences of the United States of America* 97(12):6826–31.

Chang, Jennifer L., Anthony J. Hinrich, Brandon Roman, Michaela Norrbom, Frank Rigo, Robert A. Marr, Eric M. Norstrom, and Michelle L. Hastings. 2018. “Targeting Amyloid-β Precursor Protein, APP, Splicing with Antisense Oligonucleotides Reduces Toxic Amyloid-β Production.” *Molecular Therapy* 26(6):1539–51. doi: 10.1016/j.ymthe.2018.02.029.

Chen, Xu-Qiao, and William C. Mobley. 2019. “Exploring the Pathogenesis of Alzheimer Disease in Basal Forebrain Cholinergic Neurons: Converging Insights From Alternative Hypotheses.” *Frontiers in Neuroscience* 13:446. doi: 10.3389/fnins.2019.00446.

Clary, D. O., G. Weskamp, L. R. Austin, and L. F. Reichardt. 1994. “TrkA Cross-Linking Mimics Neuronal Responses to Nerve Growth Factor.” *Molecular Biology of the Cell* 5(5):549–63.

Colcher, David, Robert Bird, Mario Roselli, Karl D. Hardman, Syd Johnson, Sharon Pope, Steven W. Dodd, Michael W. Pantoliano, Diane E. Milenic, and Jeffrey Schlom. 1990. “In Vivo Tumor Targeting of a Recombinant Single-Chain Antigen-Binding Protein.” *JNCI: Journal of the National Cancer Institute* 82(14):1191–97. doi: 10.1093/jnci/82.14.1191.

Crooke, Stanley T., Joseph L. Witztum, C. Frank Bennett, and Brenda F. Baker. 2018. “RNA-Targeted Therapeutics.” *Cell Metabolism* 27(4):714–39. doi: 10.1016/j.cmet.2018.03.004.

Dowdy, Steven F. 2017. “Overcoming Cellular Barriers for RNA Therapeutics.” *Nature Biotechnology* 35(3):222–29. doi: 10.1038/nbt.3802.

Farias, Santiago E., Pavel Strop, Kathy Delaria, Meritxell Galindo Casas, Magdalena Dorywalska, David L. Shelton, Jaume Pons, and Arvind Rajpal. 2014. “Mass Spectrometric Characterization of Transglutaminase Based Site-Specific Antibody–Drug Conjugates.” *Bioconjugate Chemistry* 25(2):240–50. doi: 10.1021/bc4003794.

Fu, Hongjun, John Hardy, and Karen E. Duff. 2018. “Selective Vulnerability in Neurodegenerative Diseases.” *Nature Neuroscience* 21(10):1350–58. doi: 10.1038/s41593-018-0221-2.

Hammond, Suzan M., Annemieke Aartsma-Rus, Sandra Alves, Sven E. Borgos, Ronald A. M. Buijsen, Rob W. J. Collin, Giuseppina Covello, Michela A. Denti, Lourdes R. Desviat, Lucía Echevarría, Camilla Foged, Gisela Gaina, Alejandro Garanto, Aurelie T. Goyenvalle, Magdalena Guzowska, Irina Holodnuka, David R. Jones, Sabine Krause, Taavi Lehto, Marisol Montolio, Willeke Van Roon-Mom, and Virginia Arechavala-Gomeza. 2021. “Delivery of Oligonucleotide-Based Therapeutics: Challenges and

Opportunities." *EMBO Molecular Medicine* 13(4):e13243. doi: 10.15252/emmm.202013243.

Jain, Nareshkumar, Sean W. Smith, Sanjeevani Ghone, and Bruce Tomczuk. 2015. "Current ADC Linker Chemistry." *Pharmaceutical Research* 32(11):3526–40. doi: 10.1007/s11095-015-1657-7.

Juliano, Rudolph L. 2016. "The Delivery of Therapeutic Oligonucleotides." *Nucleic Acids Research* 44(14):6518–48. doi: 10.1093/nar/gkw236.

Kole, Ryszard, Adrian R. Krainer, and Sidney Altman. 2012. "RNA Therapeutics: Beyond RNA Interference and Antisense Oligonucleotides." *Nature Reviews. Drug Discovery* 11(2):125–40. doi: 10.1038/nrd3625.

Lane, C. A., J. Hardy, and J. M. Schott. 2018. "Alzheimer's Disease." *European Journal of Neurology* 25(1):59–70. doi: 10.1111/ene.13439.

Panowski, Siler, Sunil Bhakta, Helga Raab, Paul Polakis, and Jagath R. Junutula. 2014. "Site-Specific Antibody Drug Conjugates for Cancer Therapy." *MAbs* 6(1):34–45. doi: 10.4161/mabs.27022.

Perez, Heidi L., Pina M. Cardarelli, Shrikant Deshpande, Sanjeev Gangwar, Gretchen M. Schroeder, Gregory D. Vite, and Robert M. Borzilleri. 2014. "Antibody–Drug Conjugates: Current Status and Future Directions." *Drug Discovery Today* 19(7):869–81. doi: 10.1016/j.drudis.2013.11.004.

Roberts, Thomas C., Robert Langer, and Matthew J. A. Wood. 2020. "Advances in Oligonucleotide Drug Delivery." *Nature Reviews. Drug Discovery* 19(10):673–94. doi: 10.1038/s41573-020-0075-7.

Salehi, Ahmad, Jean-Dominique Delcroix, Pavel V. Belichenko, Ke Zhan, Chengbiao Wu, Janice S. Valletta, Ryoko Takimoto-Kimura, Alexander M. Kleschevnikov, Kumar Sambamurti, Peter P. Chung, Weiming Xia, Angela Villar, William A. Campbell, Laura Shapiro Kulnane, Ralph A. Nixon, Bruce T. Lamb, Charles J. Epstein, Gorazd B. Stokin, Lawrence S. B. Goldstein, and William C. Mobley. 2006. "Increased App Expression in a Mouse Model of Down's Syndrome Disrupts NGF Transport and Causes Cholinergic Neuron Degeneration." *Neuron* 51(1):29–42. doi: 10.1016/j.neuron.2006.05.022.

Sang, Hua, Ning Wan, Gaoyuan Lu, Yang Tian, Guangji Wang, and Hui Ye. 2020. "Conjugation Site Analysis of Lysine-Conjugated ADCs." Pp. 235–50 in *Antibody-Drug Conjugates: Methods and Protocols*, *Methods in Molecular Biology*, edited by L. N. Tumey. New York, NY: Springer US.

Schliebs, Reinhard, and Thomas Arendt. 2011. "The Cholinergic System in Aging and Neuronal Degeneration." *Behavioural Brain Research* 221(2):555–63. doi: 10.1016/j.bbr.2010.11.058.

Selkoe, Dennis J., and John Hardy. 2016. "The Amyloid Hypothesis of Alzheimer's Disease at 25 Years." *EMBO Molecular Medicine* 8(6):595–608. doi: 10.15252/emmm.201606210.

Senechal, Yann, Peter H. Kelly, John F. Cryan, Francois Natt, and Kumlesh K. Dev. 2007. "Amyloid Precursor Protein Knockdown by SiRNA Impairs Spontaneous Alternation in Adult Mice." *Journal of Neurochemistry* 102(6):1928–40. doi: 10.1111/j.1471-4159.2007.04672.x.

Sofroniew, Michael V., Charles L. Howe, and William C. Mobley. 2001. "Nerve Growth Factor Signaling, Neuroprotection, and Neural Repair." *Annual Review of Neuroscience* 24(1):1217–81. doi: 10.1146/annurev.neuro.24.1.1217.

Strop, Pavel. 2014. "Versatility of Microbial Transglutaminase." *Bioconjugate Chemistry* 25(5):855–62. doi: 10.1021/bc500099v.

Sugo, Tsukasa, Michiko Terada, Tatsuo Oikawa, Kenichi Miyata, Satoshi Nishimura, Eriya Kenjo, Mari Ogasawara-Shimizu, Yukimasa Makita, Sachiko Imaichi, Shumpei Murata, Kentaro Otake, Kuniko Kikuchi, Mika Teratani, Yasushi Masuda, Takayuki Kamei, Shuichi Takagahara, Shota Ikeda, Tetsuya Ohtaki, and Hirokazu Matsumoto. 2016. "Development of Antibody-SiRNA Conjugate Targeted to Cardiac and Skeletal Muscles." *Journal of Controlled Release: Official Journal of the Controlled Release Society* 237:1–13. doi: 10.1016/j.jconrel.2016.06.036.

Thinakaran, Gopal, and Edward H. Koo. 2008. "Amyloid Precursor Protein Trafficking, Processing, and Function." *The Journal of Biological Chemistry* 283(44):29615–19. doi: 10.1074/jbc.R800019200.